Structural basis of Qng1-mediated salvage of the micronutrient queuine from queuosine-5′-monophosphate as the biological substrate

Shr-Hau Hung [1,7], **Gregory I. Elliott** [1], **Thakku R. Ramkumar** [2], **Lyubomyr Burtnyak**[3], **Callum J. McGrenaghan**[3], **Sana Alkuzweny**[1], **Samia Quaiyum**[2], **Dirk Iwata-Reuyl** [4], **Xiaobei Pan** [5], **Brian D. Green**[5], **Vincent P. Kelly** [3], **Valérie de Crécy-Lagard** [2,6] and **Manal A. Swairjo** [1,7,*]

[1]Department of Chemistry and Biochemistry, San Diego State University, San Diego, CA, USA, [2]Department of Microbiology and Cell Science, University of Florida, Gainesville, FL, USA, [3]School of Biochemistry and Immunology, Trinity Biomedical Sciences Institute, Trinity College Dublin, Dublin 2, Ireland, [4]Department of Chemistry, PO Box 751 Portland State University, Portland, OR 97207, USA, [5]School of Biological Sciences, Institute for Global Food Security, Queen's University Belfast, Belfast, UK, [6]University of Florida Genetics Institute, Gainesville, FL 32610, USA and [7]The Viral Information Institute, San Diego State University, San Diego, CA, USA

ABSTRACT

Eukaryotic life benefits from—and ofttimes critically relies upon—the *de novo* biosynthesis and supply of vitamins and micronutrients from bacteria. The micronutrient queuosine (Q), derived from diet and/or the gut microbiome, is used as a source of the nucleobase queuine, which once incorporated into the anticodon of tRNA contributes to translational efficiency and accuracy. Here, we report high-resolution, substrate-bound crystal structures of the *Sphaerobacter thermophilus* queuine salvage protein Qng1 (formerly DUF2419) and of its human ortholog QNG1 (C9orf64), which together with biochemical and genetic evidence demonstrate its function as the hydrolase releasing queuine from queuosine-5′-monophosphate as the biological substrate. We also show that QNG1 is highly expressed in the liver, with implications for Q salvage and recycling. The essential role of this family of hydrolases in supplying queuine in eukaryotes places it at the nexus of numerous (patho)physiological processes associated with queuine deficiency, including altered metabolism, proliferation, differentiation and cancer progression.

GRAPHICAL ABSTRACT
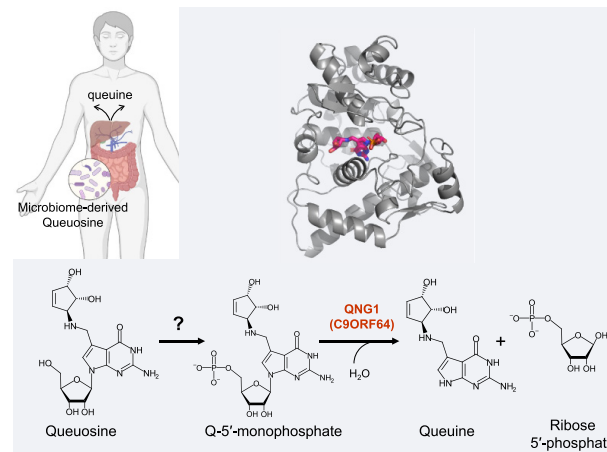
INTRODUCTION

Queuosine (Q) is a modified nucleoside found in most bacteria and eukarya at the wobble position (position 34) of tRNAs containing $G_{34}U_{35}N_{36}$ anticodons (isoacceptors for Tyr, Asp, Asn, His) (Figure 1A) ([1]). Structurally, Q comprises a cyclopentenediol ring and aminomethyl sidechain appended to a 7-deazaguanosine core ([2],[3]). In most bacteria, Q is biosynthesized *de novo*, and the pathway has been fully elucidated in *Escherichia coli* ([4]). In eukaryotes, Q-biosynthetic enzymes are absent. Therefore, this molecule

*To whom correspondence should be addressed. Tel: +1 619 206 3864; Fax: +1 619 594 4634; Email: mswairjo@sdsu.edu
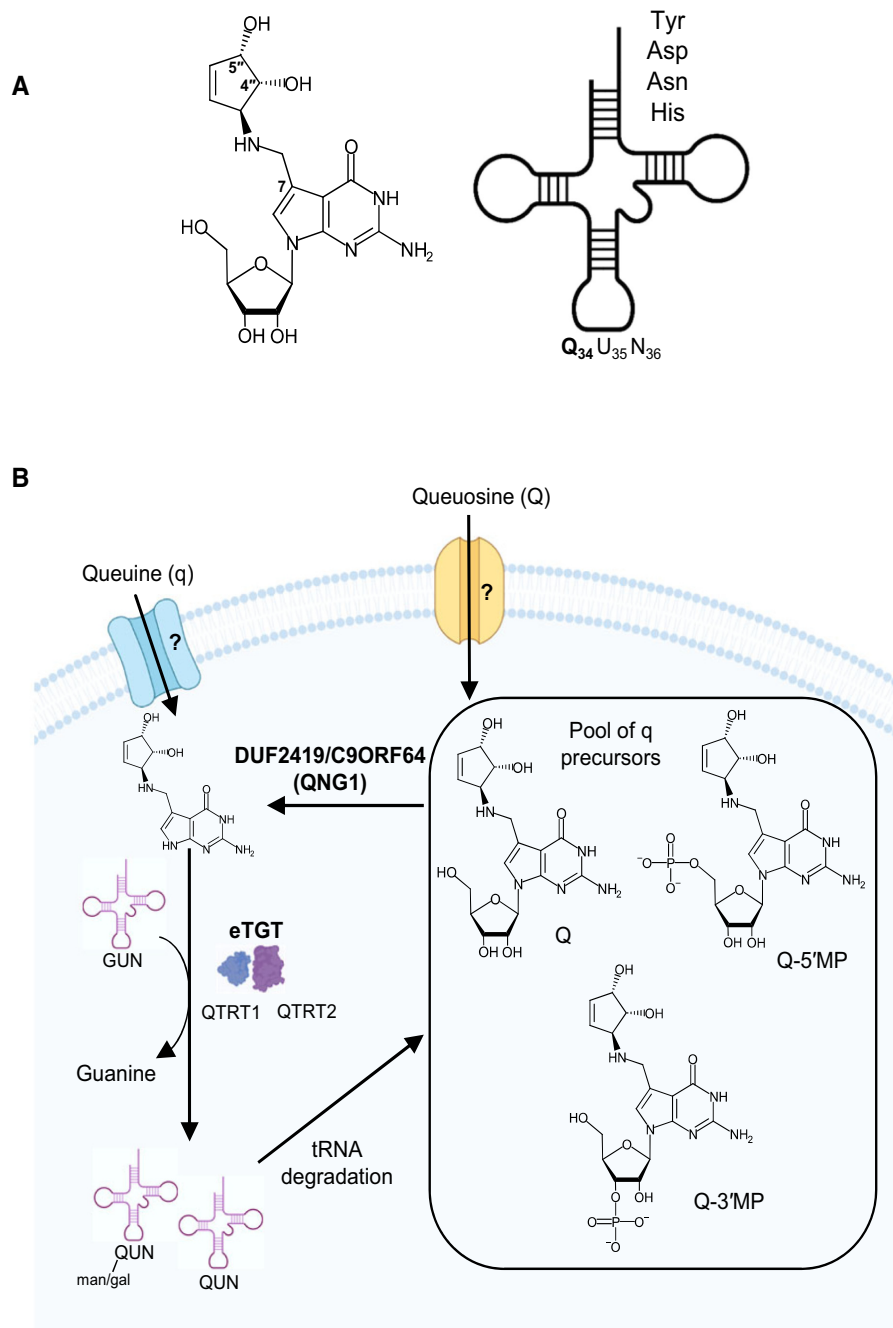
Figure 1. Queuine salvage by eukaryotic cells. (**A**) Queuosine structure and its location in bacterial and eukaryotic tRNAs carrying GUN anticodons (tyrosyl-, aspartyl-, asparaginyl- and histidyl-tRNA). (**B**) Current model for queuine uptake, incorporation in tRNA and salvage in the eukaryotic cell. Queuine (q) can be salvaged directly from the extracellular space, or alternatively from exogenous queuosine nucleoside (Q) *via* the recently discovered DUF2419 (C9orf64)-dependent pathway, incorporated into tRNA by the eTGT (comprised of QTRT1 and QTRT2 subunits) and further modified with mannose and galactose by unknown sugar transferases. Both q and Q enter the cell *via* unknown transporters, with early studies suggesting that imported queuosine may be converted to the 5′-nucleotide. Salvage of the queuine base from tRNA turnover could occur from Q, queuosine-5′-monophosphate (Q-5′MP) or queuosine-3′-monophosphate (Q-3′MP). The exact biochemical function of DUF2419 has remained unknown.

must be sourced from ingested food and/or the microbiota, and metabolized to its corresponding nucleobase, queuine (q), before incorporation into cytoplasmic and mitochondrial tRNAs (1,5–7). The incorporation reaction involves the exchange of the genetically encoded guanine at position 34 of tRNA with queuine and is catalyzed by the eukaryotic tRNA-guanine transglycosylase enzyme (eTGT), comprising a catalytic subunit (QTRT1) and a regulatory partner subunit (QTRT2) (8) (Figure 1B). In eukaryotes, Q-modified aspartyl and tyrosyl tRNAs can be further glycosylated at the C4″ hydroxyl of the cyclopentenediol ring with mannose and galactose to form manQ and galQ, respectively, by yet unidentified enzymes (9–11).

Q is the only eukaryotic tRNA modification that relies upon the supply of an exogenous substrate. A number of intriguing physiological roles for this micronutrient have emerged. For example, in mice and human HepG2 liver cells, the absence of Q in tRNA affects tetrahydrobiopterin (BH4) production, resulting in a compromised ability to produce tyrosine from phenylalanine (12). Given that BH4 is a critical cofactor for the production of numerous biogenic amine neurotransmitters, including dopamine, serotonin, epinephrine, norepinephrine and the gaseous messenger nitric oxide, a neuro-(patho)physiology role for Q has been speculated (13). Indeed, queuine is enriched in the brain (14), and axenic mice co-deficient in queuine and tyrosine present with neurological abnormalities (seizures, lethargy, staggered walking) and ultimately death within 18 days, symptoms that are reversed by the re-administration of queuine or tyrosine alone (15). Recently, the neuroprotective role of queuine has been demonstrated in *in vitro* models of Parkinson's Disease and in acute and chronic models of Alzheimer's Disease (16), highlighting its therapeutic potential in neurological disorders. In this regard, Q may bridge ancient lines of communication along the gut-brain axis.

Other Q-related metabolic changes have also been observed. Q-deficient HeLa cells demonstrate a cancer-like Warburg metabolism characterized by elevated glycolysis, glutaminolysis and lactate dehydrogenase (LDH) activity (17), in agreement with mitochondrial and LDH changes seen in other cells and organisms (18,19). These metabolic changes may be developmentally relevant since both LDH activity and the metamorphosis of slime mold *D. discoideum* and of *D. melanogaster* are accompanied by dramatic changes in the Q-modification status of tRNA (20). In addition to changes in metabolism and differentiation, Q-modified tRNA is deficient in a wide range of blood and solid cancers (21–23), and the Q-modification status of tRNA has been linked to the grade of malignancy and patient survival (22,23). The observation that tRNA in rapidly-proliferating cells is hypomodified with respect to Q led to the development of queuine analogues that could induce complete remission of multiple sclerosis in an animal model (24).

Although the eTGT-dependent incorporation of q in eukaryotic tRNA has been well characterized (25–27), little is known about the molecular mechanisms of its salvage from the extracellular space or its recycling from intracellular pools. Pioneering studies in human cells revealed highly specific q/Q membrane transporters, but their identities remain unknown (28,29). Q-5′-phosphate, Q-3′-phosphate and Q are all postulated intermediates in the intracellular salvage pathway, arising intracellularly from the normal turnover of Q-containing-tRNA (Figure 1) (30–32). This, together with early studies in algae, implied the existence of unidentified but specific nucleosidases that release q from nucleoside precursors to make it available for its incorporation into tRNA by eTGT (32,33). More recently, comparative genomic analysis of genes that co-distribute with QTRT1 led to the discovery of DUF2419 (domain of unknown function 2419) as a protein family required for q salvage in *Schizosaccharomyces pombe* (34). Yeast complementation studies showed that this role is shared by the human homolog C9orf64, and the homolog from *Sphaerobacter thermophilus*; bacteria that lack the canonical genes for *de novo* Q biosynthesis and must therefore, like eukaryotes, salvage q from the environment. Consistent with a role for Q in differentiation, C9orf64 has recently been linked to the efficient generation of induced pluripotent stem cells, being the top incompletely silenced gene during stem cell reprogramming (35), and it is among a group of possible tumor suppressor genes on the long arm of chromosome 9 commonly deleted in acute myeloid leukemia (36). Although predicted structural similarity of DUF2419 with 8-oxoguanine DNA glycosylases suggested a hydrolase role (34), its exact biochemical function in q salvage remained unknown.

Recently, two groups reported a weak *in vitro* activity of DUF2419 from *S. pombe* (37) and from the human parasite *Entamoeba histolytica (38)*, that converts queuosine to queuine, and one assigned it the function of 'queuosine nucleoside glycosylase.' Here, we report comprehensive functional, structural and biochemical characterization of *S. thermophilus* and human DUF2419, and show with *in vitro* and *in vivo* evidence that DUF2419 is a queuosine-nucleotide N-glycosylase/hydrolase (Qng1 for the bacterial enzyme, and QNG1 for the mammalian ortholog C9orf64), that releases q from Q-5′-monophosphate as the biological substrate, and this activity is required for the salvage of q from exogenous Q by *S. pombe* and human cells. Notably, in human cells Q-5′-monophosphate accumulates intracellularly in the absence of QNG1, indicating intracellular conversion of imported Q to the 5′-nucleotide by an unidentified kinase. The high-resolution substrate-bound structures, combined with complementation of a *qng1Δ S. pombe* strain with structure-guided mutants delineate the catalytic residues and strongly support a DNA-glycosylase-like mechanism for the Qng1-catalyzed reaction.

MATERIALS AND METHODS

Mice

Adult C57BL/6J mice (12 weeks of age for both sexes) were bred in specific pathogen-free conditions in individually ventilated cages (Tecniplast Green Line) and fed *ad libitum* with standard chow diet (PicoLab rodent diet 20). Studies were conducted under license from the Health Products Regulatory Authority (AE19136-P086), with prior approval from Trinity College Dublin Animal Research Ethics Committee.

HeLa cell culture

HeLa cells were purchased from the European Collection of Cell Cultures (ECACC), grown in an atmosphere of 5% CO_2 at 37°C and routinely maintained in Dulbecco's Modified Eagle's Medium (DMEM) media containing 10% fetal bovine serum (Sigma), 1.5 mM L-glutamine (Gibco), 1% penicillin/streptomycin (Gibco), except for studies evaluating q/Q salvage, where cells were grown in OptiPro™ Serum-free media (Gibco) supplemented with 2 mM L-glutamine for three or more passages before experiments. Chemically synthesized q was a gift from Dr. Susumu Nishimura (Tsukuba University, Japan) or purchased from Epitoire (Singapore). Queuosine was purchased from Epitoire (Singapore).

S. pombe strains and plasmids

The haploid *S. pombe* strains WT, *qtrt1Δ* (SPAC1687.19cΔ), *qng1Δ* (formerly *duf2419Δ* / SPAC589.05cΔ) were acquired from Bioneer, Inc. (39) and described previously (34). For Q/q salvage assays, *S. pombe* strains were grown in YES media (39) at 30°C. Chemically synthesized queuosine or queuine (both from Epitoire, Singapore), or 1% Bacto™ Peptone (as a queuosine source, BD Difco, Fisher Scientific Inc.) were added as needed. All plasmids and strains used in *S. pombe* complementation assays are listed in Supplementary Tables S1 and S2 and their construction steps and validations are explained in the Supplementary Methods and in Supplementary Figure S1. All oligonucleotides used to construct *St*Qng1 mutants used for *in vivo* complementation studies in *S. pombe* are listed in Supplementary Tables S3 and S4.

CRISPR targeting of *QNG1* gene (C9orf64) in HeLa cells

The QNG1 knock-in template was amplified by PCR from the p2attPC plasmid (Addgene ID #51547) using the forward primer 5′-GGAATATACTTCGTT CTGACACAGACGTTTCCATGGGCTCTGG CGGCGGAAGCGGAATGGCTACCGAGA AGCCCACG-3′ and the reverse primer 5′-TTCCCGGTTTCATTGAGAATCCGATGCCT CTCTTCCCATAGAGCCCACCGCATCCCCAG-3′ according to a thermocycle of 98°C for 30 s, followed by 98°C for 10 s, 72°C for 30 s for 35 cycles. Homology arms (underlined solid line) and a spacer (underlined dotted line) were introduced as overhangs into the repair-template. PCR products were purified using the QIAquick gel PCR kit (Qiagen).

A CRISPR-Cas9 targeting site was identified in the *QNG1* gene (5′-TGTGTATATGTGGGACAGCC-3′) using the CRISPOR online tool (http://crispor.tefor.net/). Equimolar concentrations (12 μM) of recombinant Cas9 protein from *S. pyogenes* (PNA Bio Ltd.) was annealed to tracrRNA and crRNA (Sigma) and delivered together with linear dsDNA repair template (3.6 μg) to HeLa cells (6×10^5) using the Neon™ Transfection System (Thermo-Fisher Scientific); 1005 V, 35 ms, 2 pulses. Electroporated cells were transferred to a 10 cm dish containing 10 ml of complete media and allowed to grow to ∼90% confluency before treatment with puromycin (3 μg/ml) for 72 h. Cells were washed with PBS twice and resistant colonies allowed to grow for a further 4–5 days. Colonies were harvested using 8 mm cloning cylinders (C3983, Sigma) and expanded for analysis.

APB-northern assay for Q-tRNA detection in *S. pombe*

A 24-h (2 ml) *S. pombe* starter culture in YES media was raised using fresh 3-day grown YES plates, and from which a 6-ml culture in YES media was initiated with OD_{600} of 0.02 and allowed to grow to OD_{600} of 2.0. Bulk *S. pombe* tRNA extraction was performed using the PurLink™ miRNA isolation kit (Thermo Fisher Scientific Inc.) and TRIzol™ reagent (Thermo Fisher Scientific Inc.). The tRNA samples (600 ng) were separated on 8 M urea-PAGE gel supplemented with 10% APB (N-acryloyl-3-aminophenylboronic acid; Sigma-Aldrich. Co.) in $1\times$ TAE buffer. Migrated tRNAs were transferred onto Biodyne™ B nylon membranes (Thermo Fisher Scientific Inc) using a wet transfer apparatus in $1\times$ TAE at 150 mA at 4°C for 90 min. After the transfer, the membrane was irradiated in a UV Crosslinker (Fisher FB-UVXL-1000, Thermo Fisher Scientific, Waltham, MA, USA) at a preset UV energy dosage of 120 mJ/cm^2. The *S. pombe* $tRNA^{Asp}_{GUC}$ was detected with the North2South Chemiluminescent Hybridization and Detection Kit (Thermo Fisher Scientific, Waltham, MA, USA). The initial membrane blocking was performed using DIG Easy Hyb reagent (Roche, Basel, Switzerland) because it drastically limits the background noise compared to the membrane blocking buffer supplied with the North2South kit (Thermo Fisher Scientific, Waltham, MA, USA). Hybridization was done at 55°C with *S. pombe* $tRNA^{Asp}_{GUC}$-specific biotinylated probe (5′-GCACGTGACAGGCTTG-3′) (Qiagen) at 0.3 μM final concentration. Final probe detection on the membrane was performed using the iBright FL1000 Imaging System (Thermo Fisher Scientific Inc.). Similar methods used to quantify Q-tRNA in HeLa cells are described in Supplementary Methods.

Cloning of wild-type proteins for *in vitro* studies

Prof. Gaetano T. Montelione (Rutgers University, Piscataway, NJ, USA) provided pET21_NESG plasmid derivatives containing the synthesized *H. sapiens* QNG1 coding sequence (plasmid HR5270-1-341-21.6) or *S. thermophilus* DSM 20745 Qng1 (Sthe_2331) recoded sequence (GenScript USA Inc., plasmid PeR1-21.1). The corresponding gene sequences are provided in the Supplementary Table S5. The *S. thermophilus* gene was PCR amplified from PeR1-21.1 using the primer set *St*Qng1_pet28_F and *St*Qng1_pet28_R, respectively (Supplementary Table S6), and subcloned into the NcoI (5′-end) and XhoI (3′-end) of pET28b to give plasmid pRGZ355. To produce Qng1 constructs with cleavable 6x-Histidine tags, the *Hs*QNG1 and *St*Qng1 genes were PCR-amplified from plasmids HR5270-1-341–21.6 and pRGZ355 using primer sets *St*Qng1subclone and *Hs*QNG1subclone (Supplementary Table S6), respectively. The genes were each subcloned into the NdeI (5′-end) and XhoI (3′-end) restriction sites of a pET28a expression vector (Novagen, San Diego CA), in frame with the N-terminal His$_6$ tag and thrombin cleavage site, using the NEBuilder® HiFi DNA Assembly Cloning Kit (New England BioLabs). The nucleotide sequences of

the resulting constructs, MAS03J1 and MAS03J2, were confirmed by Sanger sequencing (Genewiz, Inc., NJ, USA).

Mutagenesis of *St*Qng1 for crystallographic studies

Point mutagenesis was carried out on *St*Qng1 using the Q5® Site-Directed Mutagenesis Kit (New England Biolabs Inc.) and plasmid VDC3994 as the PCR template. Ile176 was mutated to Met (ATT → ATG) and Lys199 to Cys (AAA → TGC) to generate single-mutant constructs. All primer sets used for cloning and mutagenesis and the resulting constructs are listed in Supplementary Tables S6 and S7, respectively.

Protein production for crystallography and enzyme assays

Proteins were overexpressed in *E. coli* C41 (DE3) cells (Lucigen Corporation, WI, USA). Cultures were grown in Luria broth (LB) at 37°C with shaking to an optical density A_{600} of 0.5–0.6. For *St*Qng1, expression was induced by addition of isopropyl β-D-1-thiogalactopyranoside (IPTG) to a final concentration of 0.5 mM, followed by 4 h of growth. For *Hs*QNG1, the culture was cooled on the ice for 15 min with gentle mixing before induction with IPTG and subsequent incubation overnight at 18°C with shaking. Cells were harvested by centrifugation at 6000 × g for 10 min at 4°C. The cell pellet was flash-frozen in liquid nitrogen and stored at a –20°C until the protein purification procedure.

All proteins were purified by Ni-NTA chromatography followed by size-exclusion chromatography (SEC). Briefly, cell pellet from 1-liter culture was suspended and lysed in 50 ml buffer containing 50 mM Tris–HCl (pH 7.0), 300 mM NaCl, 10 mM imidazole, 5% glycerol, 1 mM β-mercaptoethanol (BME), and half a tablet of cOmplete™ ULTRA protease inhibitor cocktail (Roche Diagnostics, IL, USA; Buffer A). The cell lysates were centrifuged at 23 000 × g for 45 min at 4°C, and the supernatant loaded onto a gravity column containing 3 ml His60 Ni Superflow Resin (Takara Bio USA, Inc.), pre-equilibrated with Buffer A. The column was washed with 50 ml of Buffer A, followed by 50 ml of Buffer A modified to 500 mM NaCl and 20 mM imidazole, followed by 50 ml of Buffer A modified to 200 mM NaCl and 20 mM imidazole. The protein was eluted in Buffer A modified to 200 mM NaCl and 400 mM imidazole. The elution fractions were pooled and subjected to SEC using a BioRad NGC chromatography system and an ENrich™ SEC 650 10 × 300 column (Biorad) pre-equilibrated with 50 mM Tris (pH 7.0), 50 mM KCl and 1 mM dithiothreitol (DTT). For proteins used in enzyme assays (constructs MAS03J1 and MAS03J2), the His$_6$ tag was removed before the final SEC step as follows. The 15-ml Ni-NTA eluate was concentrated to 1 ml in an Amicon™ Ultra-15 centrifugal filter unit (30 kDa, MilliporeSigma™), and exchanged into buffer containing 50 mM Tris–HCl (pH 7.0), 300 mM NaCl, 10 mM imidazole by two consecutive dilution and concentration steps, brought to a final concentration of 2 mg/ml and subjected to thrombin digestion (1 thrombin unit per mg of protein) for 16 h at 18°C before SEC purification. For all proteins, purity of > 95% was verified by SDS-PAGE.

Preparation of selenium-labeled protein

Because *St*Qng1 lacks methionine residues, point mutagenesis was used to introduce a single methionine residue in the wild type sequence to produce selenomethionine-containing protein for *de novo* structure determination by seleno-MAD methods. Based on naturally occurring conservative substitutions in the bacterial Qng1 proteins (Supplementary Figure S2), residue I176 was selected for point mutagenesis to methionine. To produce selenomethionine-labelled protein, the *St*Qng1-I176M mutant (construct MAS03G5 containing non-removable C-terminal His$_6$ tag) was overexpressed in *E. coli* C41(DE3) in M9 minimal media (Molecular Dimensions) supplemented with L-selenomethionine, and additional amino acids to suppress endogenous methionine biosynthesis (40). Briefly, 50 ml of overnight culture in LB media was transferred to 1-liter M9 minimal media and grown at 37°C with vigorous shaking to an optical density A_{600} of 0.6. One hundred mg each threonine, lysine hydrochloride and phenylalanine, 50 mg each leucine, isoleucine and valine, and 60 mg L-selenomethionine were then added to the culture. Following 15 minutes of incubation, protein overexpression was induced by addition of IPTG to a final concentration of 0.5 mM, followed by 6 h of growth at 37°C. Cells were harvested and the protein purified as described above.

Crystallization and crystal structure determination

Crystals of selenomethionine-labeled *St*Qng1-I176M mutant (SeMet-*St*Qng1-I176M, construct MAS03G5, C-terminal His$_6$-tag on) were grown using the vapor diffusion method in drops prepared by mixing 1 μl 10 mg/ml protein solution with 1 μl crystallization solution containing 1.1 M sodium malonate, 0.1 M HEPES (pH 7.0) and 0.5% (v/v) Jaffamine ED-2001. Crystals ∼0.2 × 0.03 mm in size grew in 7 days at 20°C. Crystals of wild-type *St*Qng1 (active enzyme, construct MAS03J2 after His$_6$-tag removal) were grown in drops containing 10 mg/ml protein, 20% PEG3350 and 0.2 M sodium thiocynate (pH 6.9). Crystals of wild-type *Hs*QNG1 (active enzyme, construct MAS03J1 after His$_6$-tag removal) in complex with q were prepared by growing apo crystals in drops containing 5 mg/ml protein, 25% PEG3350, 0.2 M NaCl and 0.1 M Bis–Tris (pH 5.5) followed by soaking in 0.5 mM queuine.

To generate crystals of *St*Qng1 (inactive enzyme, C-terminal His$_6$-tag on) in complex with substrates, the complex was formed by direct addition of an aqueous solution of Q or Q-5′MP to 10 mg/ml protein solution to a final ligand concentration of 0.5 mM, and the complex was subjected to crystallization using the same conditions mentioned above for SeMet-*St*Qng1-I176M. All crystals were cryoprotected in a solution containing crystallization reagent conditions and sucrose at 25–30% (w/v) final concentration, and flash-frozen in liquid nitrogen. X-ray diffraction data were collected at the Stanford Synchrotron Research Laboratory's (SSRL, Menlo Park, CA, USA) beamlines BL9-2 and BL12-2, equipped with Pilatus CCD detectors. Data were processed in HKL3000 (41) or XDS (42).

The *St*Qng1 *de novo* structure (Supplementary Table S8) was determined in space group P4$_1$2$_1$2 by the multi-

wavelength anomalous dispersion (MAD) method using MAD diffraction data from the SeMet-*St*Qng1-I176M crystal (construct MAS03G5, C-terminal His$_6$-tag, selenium as the anomalous scatterer), and native diffraction data from an isomorphous crystal of *St*Qng1 retaining the wild-type I176 residue (construct pRGZ355, C-terminal His$_6$-tag). Using the Phenix program suite (43), a search for heavy-atom positions using the Hyss program (44) yielded 2 Se sites in the asymmetric unit with occupancies 1.23 and 1.25. Following refinement of heavy atom positions, phases were calculated using the two sites in Phaser (45). The resulting phases were subjected to density modification in DM program (46), which increased the figure of merit (FOM) from 0.28 to 0.72, upon which the FOM-weighted protein map (FoFOM) was calculated and autotraced in AutoBuild (47). At this point, 604 residues were built, 590 of them with sidechains, accounting for 91% of the total structure. Initial structure refinement in Phenix-refine (48) yielded R-factor of 0.29. Subsequent model building, solvent fitting and refinement were conducted in coot (49) and refmac5 (v5.8) (50) against the native data set. The final structure contains the wild-type I176 residue and, for simplicity, we call it the '*St*Qng1 *de novo* structure.'

The structure of wild-type *St*Qng1 (active enzyme, His$_6$-tag removed, Table 1) apo enzyme was determined in space group P3$_1$21 by molecular replacement using the Phaser-MR program (45) in the CCP4i program suite (51) and one subunit of the refined *St*Qng1 *de novo* structure as a search model. The rotation and translation searches yielded a single solution with Log-Likelihood Gain (LLG) = 11617, crystallographic R-factor of 0.308 and representing one molecule in the asymmetric unit.

The structure of wild-type *Hs*QNG1 (active enzyme, His$_6$-tag removed, Supplementary Table S9) in complex with q was determined in space group P2$_1$ by molecular replacement using the Phaser program (45) in the Phenix program suite (43) and a model generated by AlphaFold (52) as a search model. The rotation and translation searches yielded a single solution with Log-Likelihood Gain (LLG) = 2596, crystallographic *R*-factor of 0.43 (*R*-free = 0.41) and representing two molecules in the asymmetric unit.

The structures of the C-terminally His$_6$-tagged *St*Qng1 (inactive enzyme) in complex with Q or Q-5′MP (Table 1) and His$_6$-tagged K199C mutant in complex with Q (Supplementary Table S9) were determined by direct difference Fourier methods using the *St*Qng1 *de novo* structure as a starting model. For all structures, solvent fitting and refinement were conducted in coot (49) and refmac5 (v5.8) (50).

In vitro enzyme activity assays

Initial tests of *St*Qng1/*Hs*QNG1 activity were carried out in 200 μl time-course reactions containing 10 μM *St*Qng1 or *Hs*QNG1 (with His$_6$-tags removed), 50 mM Tris pH 7.0, 100 mM NaCl, 1% (v/v) glycerol, and 50 μM synthetic Q. Time-course competition assays using synthetic Q and Q-5′MP (both purchased from Epitoire, Singapore) as competing substrates were carried out in reactions containing 2 μM enzyme and 33 μM each Q and Q-5′MP and monitored over time for 180 min. Time-course activity assays on individual substrates were carried out in similar reac-

tions containing 2 μM enzyme and 33 μM either Q or Q-5′MP and rates calculated under initial velocity conditions. The reactions were held at 50°C (for *St*Qng1) or 37°C (for *Hs*QNG1) and 30 μl aliquots were taken at the indicated time points and quenched by addition of 3 μl 70% perchloric acid followed by 3 μl 5 M K$_2$CO$_3$, centrifuged for 1 min at 3884 × g and the supernatants were subjected to LC/MS analysis. End-point activity assays using Q nucleotides derived from tRNA digests as substrates were carried out in 30 μl reactions for 1–2 h using the same buffer and temperature conditions described above but containing 50 μM *St*Qng1 or 10 μM *Hs*QNG1 (with His$_6$-tags removed) and either Q-3′MP (22.9 μM), Q-3′,5′DP (17.9 μM) or Q-5′MP (6.82 μM), quenched as described above and analyzed by LC/MS. End-point reactions on AMP, GMP, UMP and CMP 5′-nucleotides as potential substrates were carried out similarly but contained 10 μM enzyme and 100 μM nucleotide and were incubated for 120 min.

LC/MS analysis

For analysis of enzyme reactions, an Agilent 6530 QTOF coupled with an Agilent 1200 HPLC, and a separation method based on a previously established protocol (53) were utilized. An Ascentis express peptide ES-C18 column (150 mm × 4.6 mm, 2.7 μm, Supelco, Inc.) was kept at 45°C, and the injection volume was 10 μl per sample. For separation, solutions of 1% formic acid in pure water (A) and 1% formic acid in acetonitrile (B) were run at a flow rate of 0.3 ml/min. The separation was started with 98% solution A, gradually decreasing to 97% solution A over 6 min, then rapidly to 2% over 2 min, then held at 2% for an additional 2 min. The column was re-equilibrated for 13 min in 98% solution A. Data were collected for the first 14.5 min of the 23-min run. Absorbance signal was measured with a diode array detector at 260, 214 and 254 nm. The mass spectrometer was used in positive ionization mode to survey masses between 100 *m/z* and 3000 *m/z*, with a scan rate of 2 spectra/s and time of 500 ms/spectrum. The electrospray ionization parameters were: ion source at 3.5 kV, gas temperature 250°C, drying gas flow 8 l/min, nebulizer 35 psi, sheath gas temperature 250°C, sheath gas flow 11 l/min, fragmentor at 175 V, and skimmer at 65 V. Data analysis was performed using Agilent MassHunter Qualitative v10. Mass spectra of queuine compounds used in this study are shown in Supplementary Figure S3. LC-MS/MS methods for quantification of free q, Q and Q-5′MP in HeLa cell extracts and media are described in Supplementary Methods and Supplementary Table S11.

Quantification of QNG1 expression levels in mouse tissue

Mice were housed under specific pathogen-free conditions, organs recovered at 6–8 weeks of age and homogenized in ice-cold Radio-Immunoprecipitation Assay (RIPA) lysis buffer containing cOmplete™ Protease Inhibitor Cocktail (Roche). HeLa cells were washed with Phosphate Buffered Saline (PBS) and lysed in RIPA buffer. Following centrifugation at 4°C for 10 min at 16 000 × g, cytosolic supernatants were recovered and protein concentrations determined using the Pierce BCA Protein Assay kit

Table 1. X-ray data collection and structure refinement statistics for wild-type *St*Qng1 and catalytically inactive (His$_6$-tagged) *St*Qng1 in complex with Q or Q-5′MP

Data collection			
Structure	Wild-type *St*Qng1 apo	*St*Qng1 (inactive) + Q	*St*Qng1 (inactive) + Q-5′MP
PDB ID	7UK3	7U1O	7U91
Space group	$P3_121$	$P4_12_12$	$P4_12_12$
Matthew's coefficient (Å^3/Da)	4.65	2.96	2.99
Solvent content (%)	73.6	58.4	58.9
Monomers/AU	1	2	2
Beamline	BL12-2	BL12-2	BL12-2
Unit cell a, b, c (Å)	95.16, 95.16, 129.32	105.66, 105.66, 157.74	105.63, 105.63, 159.59
Wavelength (Å)	0.97946	1.03317	0.97946
Resolution (Å)[a]	42.00–2.30 (2.34–2.30)	23.00–2.35 (2.39–2.35)	50–2.39 (2.43–2.39)
Measured reflections	312 644	1 222 832	827 080
Unique reflections	30 413 (1479)	38 007 (1864)	35 946 (1733)
Completeness (%)	100 (99.9)	100 (100)	99.7 (99.5)
Multiplicity	10.3 (9.6)	32.2 (16.8)	23.0 (11.3)
R-merge	0.270 (6.626)	0.389 (4.268)	0.308 (2.688)
R-meas	0.284 (6.999)	0.395 (4.401)	0.315 (2.818)
R-pim	0.087 (2.233)	0.069 (1.055)	0.064 (0.826)
CC$_{1/2}$	0.988 (0.295)	1.001 (0.256)	0.983 (0.324)
$<I/\sigma(I)>$	9.1 (0.4)	12.0 (0.75)	10.7 (0.82)
Structure refinement			
Resolution range (Å)	41.24–2.31	22.98–2.35	47.56–2.40
No. of reflections (working/free)	24 343/1317	34 207/1790	30 242/ 1580
No. of atoms in the asymmetric unit	2724	5478	5414
Protein residues	319	641	642
Water	126	267	187
Queuosine molecules	-	2	-
Q-5′MP molecules	-	-	2
Malonate ions	-	2	-
PEG	-	-	1
No. of TLS bodies	1	2	2
R_{cryst}/R_{free}[b]	0.1518/0.1746	0.1373/0.1793	0.1268/0.1673
Deviation from ideality			
Bond length (Å)	0.006	0.005	0.007
Bond angles (°)	0.001	1.400	1.471
Ramachandran plot			
Favored & allowed (%)	99.33	99.04	98.56
Outliers (%)[c]	0.67	0.96	1.44
Wilson B factor (Å^2)	38.49	39.11	41.59

[a]Highest-resolution shell information in parentheses.
[b]R$_{free}$ was calculated with 5% of the data excluded from the refinement.
[c]Four outliers are in high temperature-factor solvent exposed loops preceded or followed by a glycine or a proline; one outlier (C74) is in a highly ordered buried loop rich in bulky aromatic residues; one (D216) is at start of a 3_{10} helix and engaged in a highly ordered salt-bridge which may distort its geometry.

(Thermo Fisher Scientific). Samples and pre-stained molecular weight markers were run on a 10% sodium dodecyl sulphate-polyacrylamide gel electrophoresis (SDS-PAGE) gel, transferred to polyvinylidene difluoride (PVDF) membrane and probed with primary antibodies to C9orf64 (abcam, ab236115) and GAPDH (G8795, Sigma) followed by the secondary horse radish peroxidase (HRP)-conjugated IgG antibodies to mouse (W4021, Promega) or rabbit (W4011, Promega) in a solution of 5% (w/v) skimmed milk powder in PBS-Tween (0.1% Tween, v/v). The membrane was imaged using a BioRad Molecular Imager Gel Doc™ XR system in chemiluminescent and colorimetric modes to capture the samples and molecular-weight markers, respectively.

RESULTS

Qng1/QNG1 is required for salvage of queuine from exogenous queuosine by *S. pombe* and human cells

Previously, the role of Qng1 in q salvage from exogenous precursors by yeast was demonstrated using a *S. pombe* *qng1*Δ mutant grown in rich media and supplied with bactopeptone as a source of precursors, and using mass spectrometry for detection of q incorporation into tRNA (34). We repeated these experiments with defined media containing synthetic Q and q, and in both cases detected Q-modified tRNA with a boronate affinity electrophoresis northern blotting (APB-Northern) assay. In this assay, tRNAs containing Q migrate more slowly on a polyacrylamide gel containing 3-(acrylamido)phenylboronic acid (APB) than tRNAs lacking the modification (54). As shown in Figure 2A, supplying exogenous Q or q resulted in q incorporation in tRNA (monitoring tRNA^{Asp}) in the wild-type *S. pombe* strain, whereas the *qng1*Δ mutant strain failed to utilize exogenous Q to modify its tRNA while retaining the ability to use q. To confirm a similar function for the QNG1 family in mammals, the human homolog (C9orf64) was inactivated in human HeLa cells by means of CRISPR-Cas9 mediated mutagenesis, through the insertion of an antibiotic-reporter gene cassette into the coding region of exon 2 (Supplementary Figure S4a,b). Homozygous mutants were confirmed by Western blotting. In agreement with observations in *S. pombe*, exogenous Q, q and bactopeptone could act as sources for Q modification of tRNA
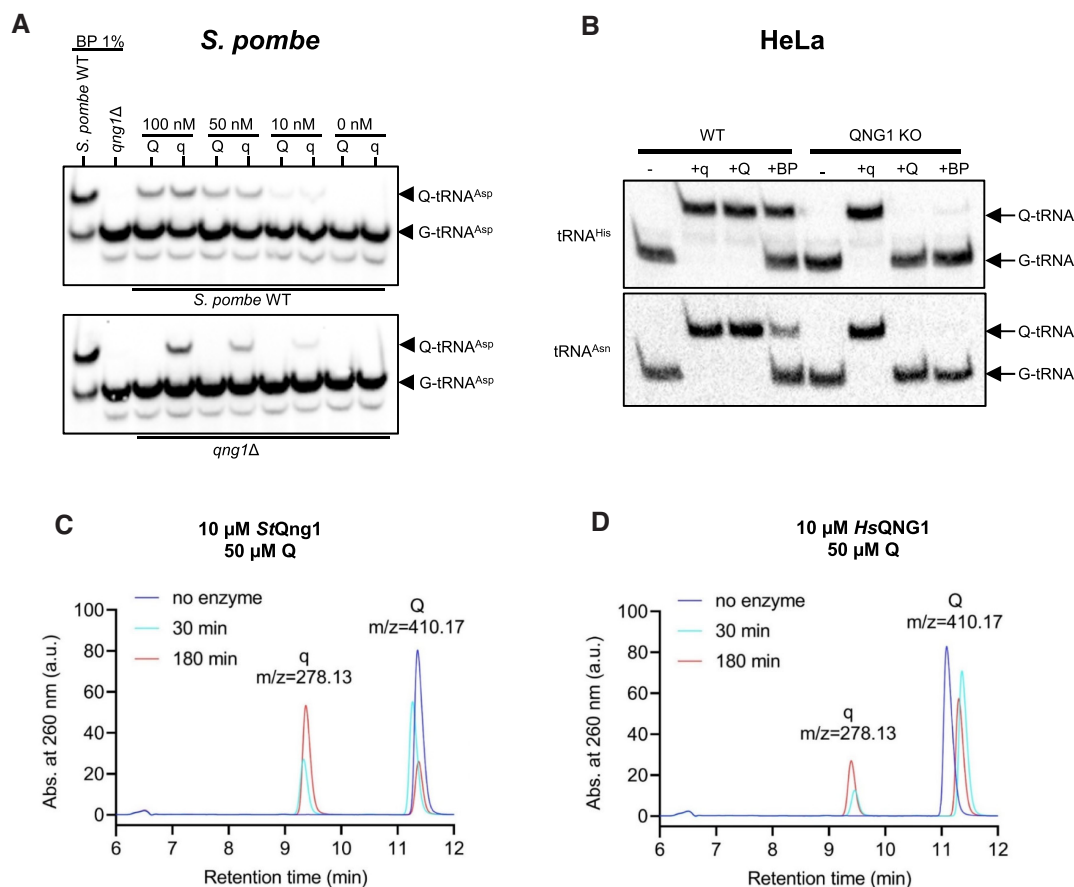
Figure 2. Qng1/QNG1-dependent q salvage from exogenous Q. (**A**, **B**) Qng1/QNG1 is required for salvage of q from exogenous Q, but not for salvage of exogenous q, by *S. pombe* and HeLa cells. (A) APB-Northern gel assay showing the queuosylation status of aspartyl tRNA extracted from *S. pombe* wild-type strain (top) and *qng1Δ* strain (bottom) grown in YES medium supplemented with 1% bactopeptone extract (BP), queuosine (Q) or queuine (q) in varying concentrations (100, 50 and 10 nM). (B) APB-Northern gel assay showing the queuosylation status of histidyl (top) and asparaginyl (bottom) tRNA extracted from wild-type and QNG1 (C9orf64)-knockout HeLa cells (CRISPR Clone 1 in Supplementary Figure S4b) grown in serum-free medium without any additions (–), or in the presence of queuine (q, 100 nM), queuosine (Q, 100 nM) or bactopeptone (BP, 1%). (**C, D**) UV absorbance traces at 260 nm from LC/MS analysis of *in vitro* time-course reactions showing release of q from synthetic Q (50 μM) in the presence of a high concentration (10 μM) of recombinant *St*Qng1 (C) or *Hs*QNG1 (D) at select time points (cyan and red lines). Active enzymes (after His$_6$ tag removal) were used. UV traces of the control reactions (no-enzyme) at the highest time point (180 min) are also shown (blue line). Reaction conditions are identical except for temperature (50°C and 37°C for the bacterial and human enzyme, respectively, based on the living environment of the source organism). The identities of the substrate and product with corresponding retention times were verified by extracting the ion counts for the expected masses $[M^+H^+] = m/z$ 278 for q and 410 for Q (Supplementary Figure S4c,d).

(determined for tRNA^{His} and tRNA^{Asn}) in wild-type cells, whereas in *QNG1* knockout cells, only q could function as a source to generate Q-modified tRNA (Figure 2B). These results show that Qng1/QNG1 is required for *S. pombe* and human cells to salvage the q base from exogenous Q, but is not required for salvage of exogenous q, consistent with the notion that Qng1/QNG1 may act as a hydrolase to release the queuine base from its ribonucleoside precursor. Indeed, we evaluated the ability of the recombinant *S. thermophilus* and human proteins (*St*Qng1 and *Hs*QNG1, respectively) to release q *in vitro* when presented with Q as substrate. Activities were measured quantitatively by monitoring Q consumption and q formation by LC/MS over time (Figure 2C, D, Supplementary Figures S4c,d and S3a,b). In the presence of either protein and under conditions of high enzyme concentrations relative to substrate (10 μM enzyme, 50 μM Q), q was produced concomitantly with the consumption of Q, indicating that Qng1/QNG1 proteins can catalyze the re-

lease of the q base directly from Q as substrate. However, further investigations described below show that Q is not the biologically relevant substrate.

Crystal structure of Qng1 reveals an HhH-fold architecture characteristic of many DNA glycosylases

To gain insight into the catalytic function of Qng1, we determined the crystal structure of wild-type *St*Qng1 at 2.31-Å resolution in the apo form (Table 1, Figure 3a and Supplementary Figure S5a). The structure reveals a monomeric protein comprising 14 α-helices and 6 β-strands distributed into N- and C-terminal lobes that enclose an active-site cleft at their interface. A DALI search for similar structures returned several DNA glycosylases of the base excision repair pathway, all of which belong to the helix–hairpin–helix (HhH) structural superfamily of DNA glycosylases. These include the archaeal and eukaryotic 8-oxoguanine glyco-
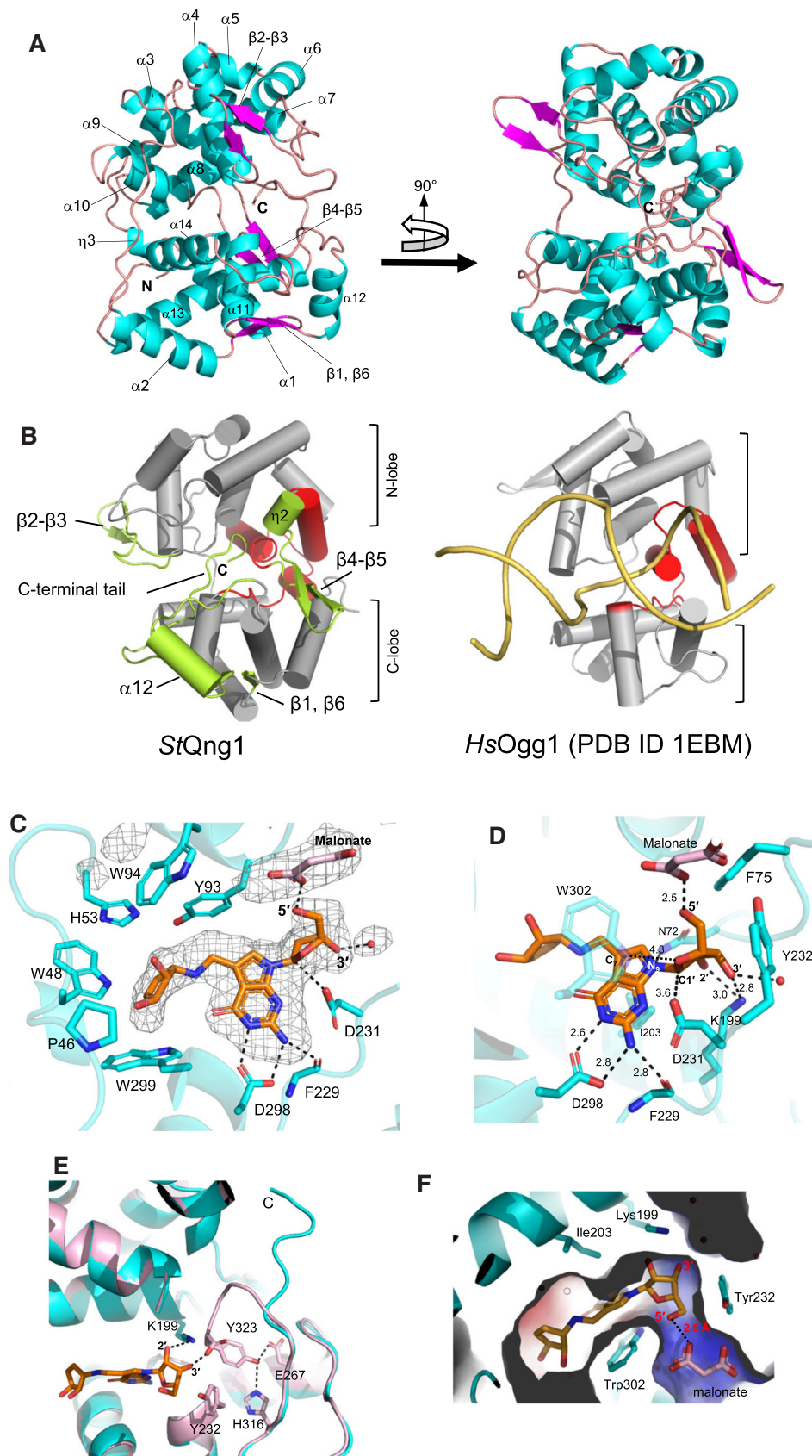
Figure 3. Qng1 structure and Q recognition. (**A, B**) Overall structure of Qng1. (A) Ribbon diagram of the *St*Qng1 monomer. Secondary structure elements are shown in different colors and labeled. The C-terminus marks the general location of the active site. (B) Comparison of the crystal structures of *St*Qng1

sylases (AGOG and Ogg1, respectively) which remove oxidized purines from DNA (55,56), and the bacterial endonuclease III (EndoIII) enzymes which remove oxidized pyrimidines and nick the backbone at the apurinic site (57). HhH-family DNA glycosylases share a two-lobe architecture and a central HhH motif, a non-specific DNA binding element consisting of two α-helices connected by an α-hairpin-loop, that serves to anchor the DNA to the protein and indirectly facilitate base-flipping to expose damaged bases in DNA (58). Structure-based multi-sequence alignment of Qng1/QNG1 with representatives of the DNA glycosylase families reveals 22% average sequence similarity (10–13% identity with individual glycosylases) and only two invariant residues, both residing in the HhH motif and critical for catalysis in HhH family DNA glycosylases (Supplementary Figure S6). These residues are an aspartate (D231 in *St*Qng1), which acts as the nucleophile that initiates glycosidic bond breakage in DNA glycosylases, and a lysine residue (K199 in *St*Qng1) shown to be critical (e.g. in human Ogg1) for specific recognition of the target nucleoside and positioning of its flipped ribose during the base hydrolysis reaction (59). While it contains an analogous HhH motif, Qng1 harbors several secondary structure insertions that flank the active site region and distinguish it from DNA glycosylases (Figure 3b and Supplementary Figure S6). These insertions are two β-hairpins β2-β3 (W76-G92 in *S. thermophilus* residue numbers) and β4-β5 (R185-Y198), the latter of which is preceded by a one-turn 3_{10} helix (η2, P182-F184) and is an insertion in the HhH motif itself; a 2-strand antiparallel β-sheet (β1 and β6, V24-D26 and L244-Y246); a 2.5-turn α-helix (α12, P248-R256) followed by an extended loop; and a 15-residue C-terminal tail (P309-Y323) that extends into and positions the C-terminal carboxylate in the active site region. These structural features, which are conserved in the Qng1/QNG1 family, cluster in and block the inter-lobe cleft available for DNA binding in DNA glycosylases. Thus, Qng1/QNG1 and HhH-family DNA glycosylases use a common ancient fold to catalyze the same reaction (base excision) on different substrates in distinct metabolic pathways.

Substrate recognition by Qng1

To elucidate how the enzyme recognizes Q, we determined the crystal structure of a C-terminally His_6-tagged, catalytically inactive *St*Qng1 construct in complex with Q at 2.35-Å resolution (Figure 3C, D, Table 1). This construct is rendered inactive due to the presence of the C-terminal His_6 tag on the protein (see below). Q is bound in a deep hydrophobic pocket with its N-glycosidic bond in an anticonformation and its C1′ atom positioned 3.6 Å from the HhH motif invariant side chain D231, strongly suggesting that D231 is the nucleophile that initiates glycosidic bond breakage, as in DNA glycosylases. The 7-deazaguanine ring is sandwiched between I203 and W302, and anchored via H-bonding of its N4 and N5 atoms with the side chain of D298, which provides additional specific recognition and discrimination against adenine. W302 and D298 are conserved in the Qng1/QNG1 family, and I203 is invariably an aliphatic residue (Supplementary Figures S2 and S7). The cyclopentenediol ring of the 7-substituent group of Q occupies a hydrophobic pocket formed largely by the conserved aromatic side chains W48, Y93, W94, W299 and by P46 and H53, with Y93 stacking face to edge in cation-π interactions with the 7-deazaguanine ring and 7-methyl-amine moiety of Q (Figure 3C). These residues form a specificity pocket that can accommodate the large 7-substituent group of Q, apparently based on size and shape compatibility, as no interactions are seen with the cyclopentenediol hydroxyl groups.

The ribose of Q adopts a C2′-endo conformation and is held in place via edge-to-face stacking against the aromatic side chains of F75 and Y232, both strictly conserved residues, and via H-bonding of its ring oxygen atom with the side-chain nitrogen of W302, and its 2′- and 3′-OH groups with the HhH-motif K199 (Figure 3D). The crystal structure of the *St*Qng1 K199C mutant bound to Q, which we determined at 2.5-Å resolution (Supplementary Table S9), shows the ribose of Q flipped ∼180° around the glycosidic bond (Supplementary Figure S5b), suggesting that K199 serves to orient the ribose in the active site for optimal positioning of its C1′ for catalysis, paralleling the role of the HhH-motif lysine in monofunctional DNA glycosylases (59).

Superposition with the wild-type apo structure shows no substrate-induced conformational changes, but reveals a functional role for the C-terminal carboxylate in recognition of the ribose moiety (Figure 3E): In the wild-type structure, the 3-residue C-terminal peptide $I_{321}FY_{323}$ adopts a bent conformation, positioning the terminal carboxylate adjacent to the active site cavity, with the ultimate side chain, Y323, stacking against Y232 (part of the ribose binding pocket) and H-bonding with E267 and H316. In the Q-bound structure, and due to the presence of the C-terminal His_6 tag on the protein, the C-terminal peptide adopts an extended conformation whereby the terminal carboxylate is pulled away from the active site. The superposition allows visualizing Q in the active site of the wild-type/active

---

(left) and of human Ogg1 (right, PDB ID 1EBM (Bruner et al., 2000)) as an example of the HhH DNA glycosylase family, showing their common two-lobe architecture and HhH motifs (red). The two lobes are indicated with brackets. DNA bound to *Hs*Ogg1 (gold) marks the general DNA binding cleft in HhH DNA glycosylases, and the Qng1-specific surface insertions (green) differentiate it from DNA glycosylases. See full structure-based sequence alignment in Supplementary Figure S6. (**C–F**) Q recognition by Qng1. (C) Omit Fo-Fc map (resolution 2.35 Å, contour level 1.5 σ) in the active site region of *St*Qng1 bound to queuosine. All residues of the cyclopentenediol binding pocket are shown in stick model. (D) View showing enzyme interactions with the 7-deazaguanine and ribose moieties of Q. Distances are in Ångstroms. (E) The terminal carboxylate is integral to the active site and catalysis. Superposition of the crystal structures of wild-type apo *St*Qng1 (active, pink) and of the His_6-tagged *St*Qng1 bound to Q (inactive, cyan) allows visualizing substrate binding in the active site of the wild-type enzyme. The C-terminal peptide in the wild-type structure is bent toward the active site, which would position the terminal carboxylate within contact distance from the ribose of Q, participating in recognition together with K199. The invariant C-terminal Tyr323 side chain is anchored by hydrogen bonds and stacking against the ribose-pocket residue Y232. (F) View of the electrostatic surface potential in the active site region showing the positively charged pocket occupied by the malonate ion near the 5′-OH of bound Q, suggesting that Q-5′MP could be a substrate for Qng. In all panels, the Q molecule and malonate ion are shown in orange and pink stick model, respectively, and water molecules are shown as red spheres.

enzyme based on its position in the Q-bound His$_6$-tagged structure, and shows the terminal carboxylate moiety, in its wild-type bent conformation, positioned within H-bonding distance from the 3′-OH of the substrate's ribose (Figure 3E). These observations, together with the strict conservation of Y323 and its interacting residues (Supplementary Figures S2 and S7), strongly suggest that the terminal carboxylate is an integral part of the active site where it serves to coordinate the ribose for productive binding, next to K199. They also explain the inactivity of all our C-terminally His$_6$-tagged Qng1 constructs.

Further, closer inspection of the electron density maps for the Q-bound structure reveals density for a malonate ion, originating from the crystallization buffer, and bound in a positively charged pocket adjacent to the ribose 5′-OH of Q (Figure 3C, F). The location of this malonate ion and its presence in the Q-bound structure but not in the apo structure suggest that it occupies a binding site for the phosphate moiety of a Q nucleotide that may also be a substrate of Qng1.

Queuosine-5′-monophosphate is the primary substrate of Qng1/QNG1

Early studies showed that cell-free extracts of Vero cells (African green monkey kidney) contain a very weak Q to q conversion activity but a robust activity that converts queuosine-5′-monophosphate (Q-5′MP) to q. These studies suggested that the latter activity was responsible for the ability of intact Vero cells to retrieve q from cellular tRNA degraded during the normal turnover process, as none of the other possible tRNA degradation products (Q, Q-3′MP, or mannosyl-Q-5′MP) allowed for the maintenance of Q-tRNA levels during q starvation (30). Further, the presence of a bound malonate ion near the 5′-OH of Q in the co-crystal structure (Figure 3f) suggests that the 5′ nucleotide of Q may also be a substrate of Qng1. We therefore tested the activities of the bacterial and human enzymes on Q-5′MP, as well as on queuosine-3′-monophosphate (Q-3′MP), and queuosine-3′,5′-diphosphate (Q-3′,5′DP) prepared from tRNA digests (see Supplementary Methods). End-point enzyme activity assays using each of these nucleotides as a substrate and high enzyme concentration showed 100% consumption of Q-5′MP, while very low activity was observed on Q-3′,5′DP (4.9% and 10% consumption by the bacterial and human enzyme, respectively) and no q production was detected when Q-3′MP was used as substrate (Figure 4A–C, Supplementary Figure S8 and Supplementary Table S10). In addition, both *St*Qng1 and *Hs*QNG1 exhibited no base excision activity on full-length *E. coli* tRNA by APB-Northern assay (Supplementary Figure S8g). Finally, a competition time-course assay conducted in the presence of both Q and Q-5′MP as competing substrates (2 μM enzyme, 33 μM each Q and Q-5′MP) showed much greater consumption of Q-5′MP than of Q by both enzymes. Specifically 70% of Q-5′MP and almost no Q was consumed by *Hs*QNG1 in the presence of Q-5′MP in the 3-h reaction time (Figure 4E and Supplementary Figure S9b,d). Likewise, 54% of Q-5′MP and only 15% of Q was consumed by *St*Qng1 in this reaction (Figure 4D and Supplementary Figure S9a,c). Further, re-

action rates measured under initial velocity conditions on the individual substrates show that both enzymes exhibit more robust activities when presented with Q-5′MP as substrate in comparison to Q (Supplementary Figure S11). The rate of q release by *St*Qng1 is 0.255 ± 0.034 μM/min and 0.146 ± 0.015 μM/min from Q-5′MP and Q, respectively, a 1.7-fold preference for Q-5′MP over Q. *Hs*QNG1 is 12-fold more active on Q-5′MP than on Q, with rates of 0.481 ± 0.043 μM/min for Q-5′MP and 0.040 ± 0.002 μM/min for Q. These results show that Q-5′MP is the primary substrate for Qng1/QNG1 and, for the human enzyme, it is the biologically relevant substrate. Further, both enzymes fail to catalyze release of the nucleobase from the 5′ nucleotides AMP, UMP, CMP or GMP (Supplementary Figure S9e–h), indicating specificity for the queuine base.

As predicted, the crystal structure of *St*Qng1 in complex with Q-5′MP (resolution 2.4 Å, Table 1) shows the nucleotide making the same interactions as the nucleoside via its 7-deazapurine and 7-substituent groups (Figure 4f). The phosphate moiety, which occupies the previously observed malonate pocket, makes electrostatic contacts with R80 and K233, and H-bonds with Y232 (water-mediated) and Q306 side chains and Y93 backbone, all either highly or strictly conserved residues in the Qng1/QNG1 family. The observed interactions of Q-5′MP with Y232 and K233 are consistent with compromised ability of *St*Qng1 variants carrying alanine substitutions at these residues to complement the Q- phenotype (absence of Q in tRNA) of the *S. pombe qng1Δ* strain when supplied with exogenous Q (Supplementary Figure S12).

HeLa cells harbouring a knockout of QNG1 accumulate intracellular Q-5′MP from exogenously supplied queuosine

Given that the utilization of exogenous Q by HeLa cells depends on QNG1 (Figure 2A, B), the observation that Q-5′MP is the primary substrate for the enzyme necessitates that Q is first phosphorylated in the cell prior to hydrolysis, as was previously suggested (30). To evaluate this possibility, we administered Q to wild-type and QNG1-knockout HeLa cells for 24 h and then quantified Q-5′MP, Q and q in the medium and intracellular extract by LC/MS (Figure 4G–I). In wild-type HeLa cells, exogenously added Q was converted to q base within the cell, the greatest proportion of which was exported back into the medium (Figure 4H), suggesting that once tRNA is fully modified with q, the excess free base is released from the cell. Notably, only low levels of Q-5′MP were detected in wild-type cells. By contrast, in QNG1-knockout cells, Q that was taken up intracellularly led to a large accumulation of Q-5′MP, but no observable levels of q (Figure 4I).

Ostensibly, a cellular kinase exists to phosphorylate queuosine, and QNG1 is the sole enzyme in HeLa cells capable of hydrolyzing the resulting nucleotide to queuine. In addition, the data demonstrate that Q-5′MP is not exported from the cell despite high levels of accumulation. It is probable that queuosine phosphorylation is mechanistically exploited by the cell to capture and prevent re-release of the molecule. Taken together, these results demonstrate that Q-
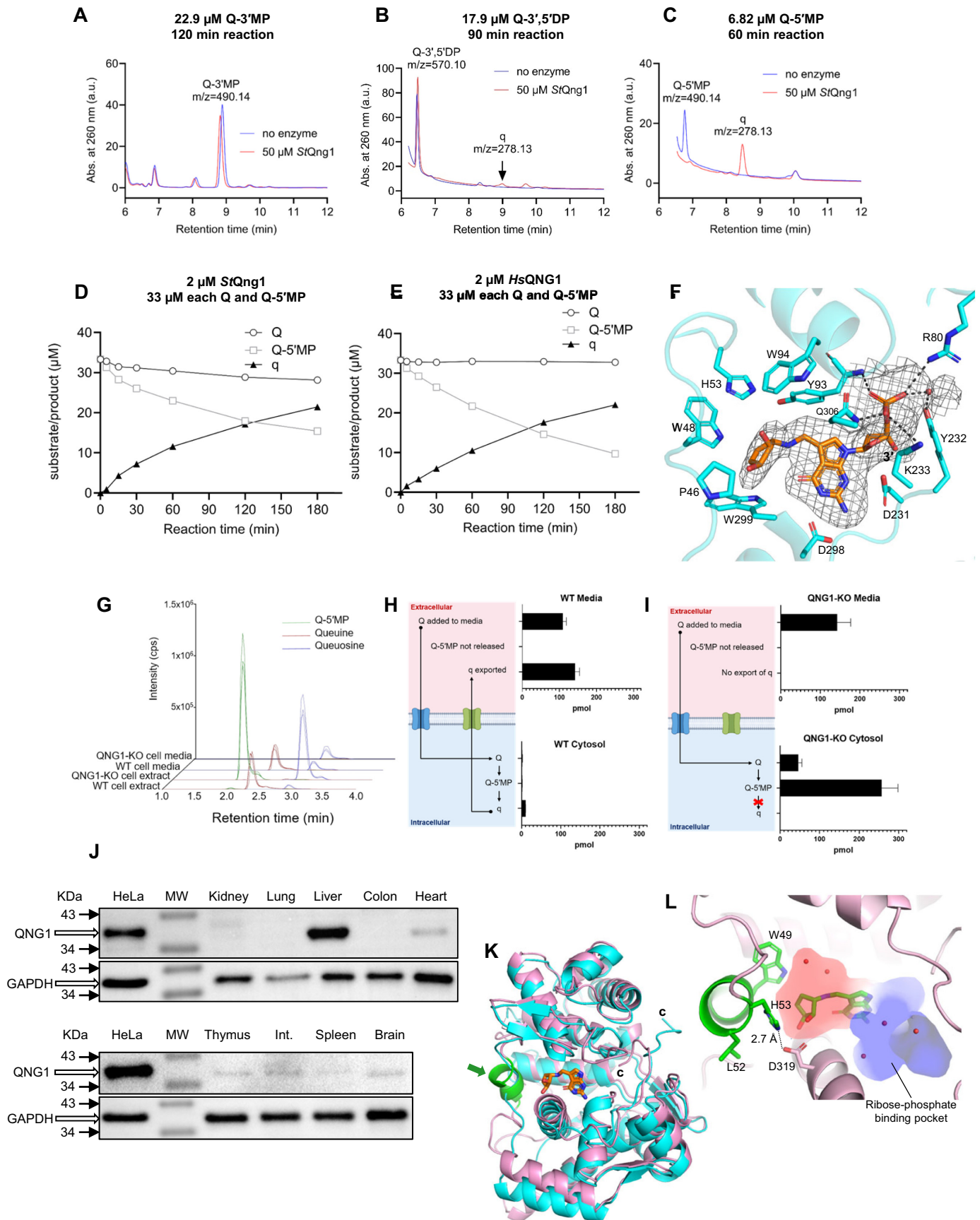
Figure 4. Q-5′-monophosphate is the biologically-relevant substrate of Qng1/QNG1. (**A–C**) LC/MS analysis of end-point *St*Qng1 reactions containing various Q nucleotides as substrates. Active enzyme (after His₆ tag removal) was used. UV absorbance traces at 260 nm from LC/MS analysis of *St*Qng1

5′MP, not Q, is the biological substrate of *Hs*QNG1, and suggest that QNG1 may also be responsible for salvage of q from intracellular pools of Q-5′MP resulting from intracellular tRNA turnover (q recycling), in addition to salvage from exogenous Q.

QNG1 is highly expressed in the mammalian liver

Given that human cells salvage q by importing Q and converting it to Q-5′MP intracellularly, we reasoned that in mammals Q is likely to be the major salvage component from the gut microbiome following the digestion and degradation of microbiome tRNA. To test this idea, we assessed QNG1 (C9orf64) expression in various tissues from adult C57BL/6 mice. Western blotting for the QNG1 protein in cytosolic supernatants of homogenized tissues showed a strong band in the liver, indicative of a high level of QNG1 expression (Figure 4J). This contrasts with the data from other organs including heart, brain, thymus, intestine and spleen, wherein only a weak band was observed, indicating that QNG1 expression is low at best given that the antibody used exhibits some non-specificity (Supplementary Figure S4b). These results strongly suggest that the liver plays a central role in the recovery of Q from the gut (through the portal vein) and its ultimate conversion to q for distribution to the rest of the body.

Crystal structure of human QNG1 suggests inability to take sugar-modified Q-5′MP as substrate

Early studies suggested that the free queuine base is salvaged by mammalian cells in the unmodified form and incorporated as such into tRNA. Specifically, studies on q salvage in Vero cells have shown that mannosyl-Q-5′MP (purified from tRNA digests) is not a substrate of the q salvage activity contained in the cell-free extracts of these cells, and that when a mixture of Q-5'MP and sugar-modified Q-5'MP is provided as substrate, no mannosyl- or galatcosyl-q was generated (30). This can be explained by the crystal structure of *Hs*QNG1 in complex with q, which we determined at 2.26-Å resolution (Supplementary Table S9. Attempts to produce co-crystals of *Hs*QNG1 with Q/Q-5′MP

were unsuccessful). *Hs*QNG1 exhibits 39% sequence identity with *St*Qng1 and shows a similar overall structure (Figure 4K, superposition r.m.s.d. 1.6 Å over 314 or 95% of C_α atoms) and a conserved active site architecture. However, *Hs*QNG1 harbors a 2-turn helix (residues V46-H53 in *Homo sapiens* sequence numbers, Supplementary Figure S7), absent in *St*Qng1, adjacent to the cyclopentenediol binding pocket (Figure 4K). This helix contributes bulky side chains and a salt bridge with the last helix in the C-terminal lobe, which constrict the pocket, rendering it too small to accommodate an O-mannosyl or O-galactosyl residue on the cyclopentenediol group of the substrate (Figure 4L). The helix is conserved in animal and fungal QNG1/Qng1 proteins (Supplementary Figure S7), suggesting that these organisms would be likewise unable to salvage sugar-modified q from exogenous glycosyl-Q precursors nor recycle it from possible endogenous glycosyl-Q-5′MP resulting from tRNA turnover.

Mechanism of the Qng1 catalyzed reaction

Qng1/QNG1 and the 8-oxoguanine DNA glycosylase Ogg1 possess similar active site architectures and purine binding pockets, with the exception of the Ogg1-specific residue that anchors the N7 atom of the base, which is missing in Qng1/QNG1, consistent with the 7-deaza structure of Q-5′MP. Two mechanisms have been proposed for cleavage of the N-glycosidic bond by HhH-family DNA glycosylases. The first proposes that hydrolysis proceeds through a double displacement mechanism that features a covalent glycosyl-enzyme intermediate that forms from nucleophilic attack of the conserved HhH-motif Asp residue (60–62). The covalent bond is then cleaved via nucleophilic attack of a water molecule at C1′, resulting in retention of stereochemistry (i.e. a product with the β-anomeric configuration). The second proposal invokes a stepwise SN1 process, wherein N-glycosyl bond cleavage yields a discrete oxocarbenium ion intermediate (63–65), followed by water addition to the ribose. The role of the conserved active site Asp in this mechanism is to stabilize the transition state leading to the oxocarbenium ion intermediate and to position

---

reactions containing 50 μM enzyme and 22.9 μM Q-3′MP (A), 17.9 μM Q-3′,5′DP (B) or 6.82 μM Q-5′MP (C) as substrates (red line), and of no-enzyme control reactions (blue line). Reaction times are 120, 90 and 60 min, respectively. Queuine release activity is robust when Q-5′MP is used as substrate (100% of Q consumed in a 60-min reaction), and absent or negligible when Q-3′MP or Q-3′,5′DP, respectively, are used as substrates (only 4.9% of Q-3′,5′MP consumed in a 90-min reaction and no Q-3′MP consumed in a 120-min reaction). Similar data for the human enzyme are shown in Supplementary Figure S8d-f and summarized in Supplementary Table S10. (**D, E**) Competition assays of *St*Qng1 and *Hs*QNG1 activities using Q and Q-5′MP as competing substrates. Substrate and product concentrations from LC/MS analysis of time-course reactions containing 2 μM *St*Qng1 (D) or *Hs*QNG1 (E) and 35 μM each Q and Q-5′MP, showing consumption of Q-5′MP, but not Q, and production of q. Time points are 5, 15, 30, 60, 120 and 180 min. Quantification was based on A_{260} peak areas in the LC chromatograms (Supplementary Figure S9a–d), normalized to the concentration of a Q standard in the no-enzyme control. Data represent triplicate reactions and errors are smaller than the displayed symbols (standard-error range ±0.05 to ±0.43 μM). (**F**) Omit Fo-Fc electron density map of *St*Qng1 bound to Q-5′MP, in the active site region (resolution 2.4 Å, contour level 3 σ). Residues of the cyclopentediol and phosphate binding pockets are shown. (**G–I**) HeLa cells harbouring a knockout of QNG1 accumulate intracellular Q-5′MP from exogenously supplied queuosine. (G) LC–MS/MS was used to quantify extracellular (Media) and intracellular (Cytosol) levels of Q, Q-5′MP and q in wild-type (WT, panel H) and QNG1-knockout HeLa cells (QNG1-KO, panel I) supplied with queuosine nucleoside (250 nM) for 24 h in the culture medium. Quantification was done using standard curves as described in Supplementary Methods (Supplementary Figure S10). (**J**) High-levels of QNG1 expression in mouse liver are consistent with a role in Q salvage from the gut. Western blot assessment of QNG1 (C9orf64) expression in HeLa cells and tissues from adult C57BL/6 mice. GAPDH serves as a loading control. MW, molecular weight markers; Int, small intestine. (**K**) Superposition of the crystal structures of wild-type *Hs*QNG1 (pink) with bound q (orange stick model) onto His6-tagged (inactive) *St*Qng1 (cyan) with bound Q-5′MP (ligand not shown). The extra helix in the human enzyme adjacent to the cyclopentenediol binding pocket is colored in green and indicated with an arrow. View is similar to panel F. (**L**) Close up view of the active site cavity in the human enzyme represented by its electrostatic surface potential, with bound q. The human-specific helix is colored in green, and bulky side chains W49 and L52 and the H53-D319 salt bridge abutting and constricting the cyclopentene binding pocket are shown in stick model. Water molecules are shown as red spheres.
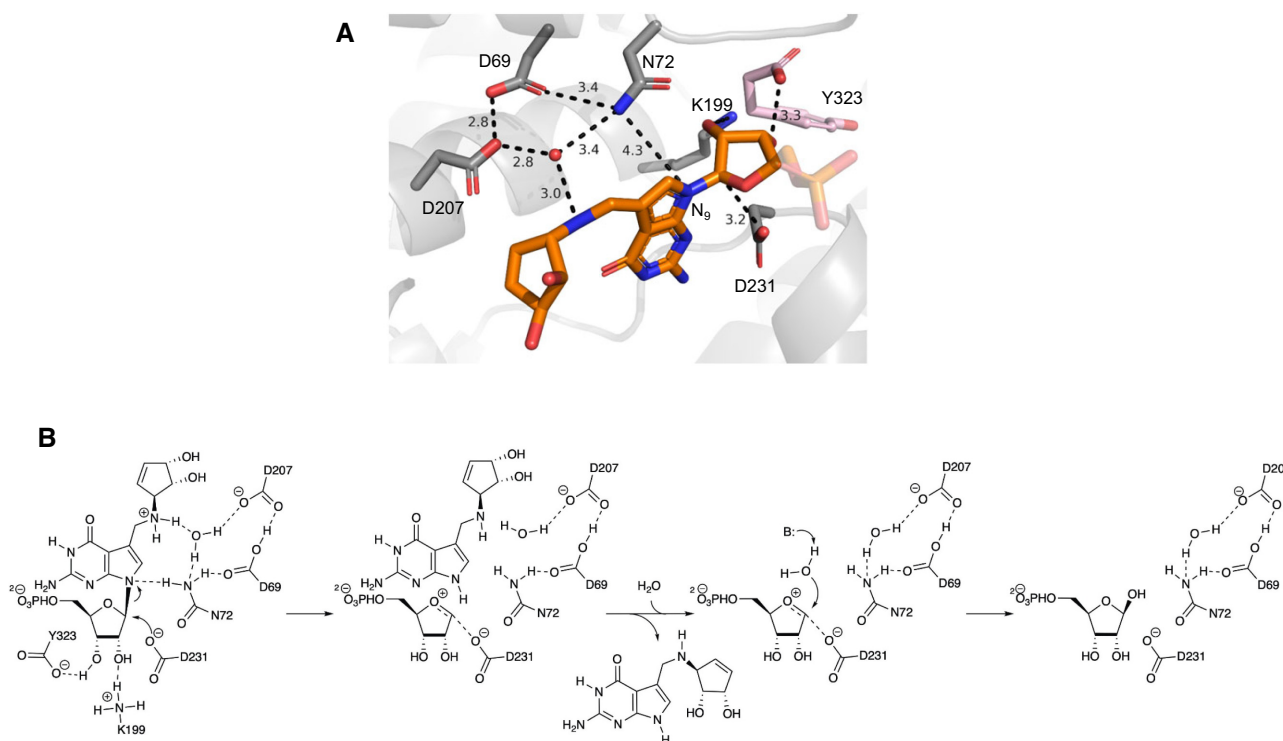
Figure 5. Proposed mechanism of the Qng1 catalyzed reaction. (**A**) View of strictly conserved H-bonding network putatively leading to protonation of the purinic N7 atom. For a complete representation of the active site as it would be in the catalytically active state, the C-terminal Y323 is modeled based on its position in the crystal structure of wild-type (active) *St*Qng1 (pink stick model). For clarity, the substrate phosphate moiety is shown in transparent stick model. (**B**) Proposed catalytic mechanism of Qng1. Our structural data argue strongly for bond cleavage and formation with retention of configuration, either *via* a covalent intermediate with D231 in a formal double-displacement mechanism, or *via* an SN1 mechanism in which D231 stabilizes the intermediate oxocarbenium ion electrostatically and water addition occurs from the same face as the departed base. These represent mechanistic extremes on a spectrum of potential reactivity, and to reflect this mechanistic ambiguity we show the reaction intermediate as possessing an extended, partial covalent bond between C1′ and D231, with partial oxocarbenium ion character. The interactions of Y323 and K199 are not shown after the first frame for clarity.

and possibly deprotonate the nucleophilic water molecule, resulting in a direct-displacement and inversion of stereochemistry at C1′, producing a product with the α-anomeric configuration.

Neither mechanism can be ruled out for Qng1 by our data (Figure 5). Given the position of the conserved HhH-motif D231, it can easily serve as a nucleophile, forming a covalent intermediate. D231 could also function purely in electrostatic stabilization of a positive oxocarbenium ion intermediate, allowing an SN1 mechanism. However, the absence of any water molecules on the underside of Q-5′MP precludes attack of water from that side or its activation by D231. Thus, a product with inverted stereochemistry at C1′ (i.e. with α-configuration) is not possible. Further, key to both mechanistic proposals is protonation of the base (at N7 of purine substrates in the case of DNA glycosylases), which facilitates glycosidic bond cleavage and allows departure of the base as the neutral species. Q-5′MP lacks N7, and as noted above, Qng1 lacks the residue that protonates this atom in the Ogg1 catalyzed reaction. Instead, the N9 atom of Q-5′MP appears to be the site of protonation, receiving the proton from the side chain of N72, which is able to function as the general acid due to its participation in a well-defined and conserved H-bonding network with D69, D206, a water molecule, and the 2°-amine of the queuosine

side chain (Figure 5), the latter of which should arrive in the active site in the protonated form. Thus, proton transfer can be thought of as originating from the 2°-amine of Q-5′MP. Notably, the water molecule in this network is the only water molecule seen in all of our Qng1/QNG1 crystal structures, trapped in the deep and otherwise hydrophobic nucleobase binding pocket. Further, the proposed putative role of D69, N72, D207 and D231 in catalysis is consistent with a compromised ability of *St*Qng1 variants carrying alanine substitutions at these residues to complement the Q-phenotype (absence of Q in tRNA) of the *S. pombe qng1Δ* strain when supplied with exogenous Q (Supplementary Figure S12).

It is notable that the substrate Q-5′MP is essentially completely enclosed in the active site, requiring that the protein undergo a significant conformational change to allow both substrate binding and product departure. While the active site is remarkably dehydrated in all our ligand bound structures, departure of the queuine product would presumably allow binding of the substrate water and generation of the abasic ribose product. Alternatively, the water molecule in the H-bonding network might serve as the substrate water, but given its spatial location and tight association with N72 and D207, we favor the entry of substrate water in concert with queuine departure.

DISCUSSION

The data presented here establish the biological function of Qng1/QNG1 as a queuosine-5'-monophosphate N-glycosylase/hydrolase. We provide *in vitro* evidence from both competition experiments (Figure 4D, E) and initial rate data (Supplementary Figure S11) that Q-5′MP is the preferred substrate, and *in vivo* evidence that in the absence of QNG1 Q-5′MP accumulates in the cell with no q produced (Figure 4G–I). The difference between the human and bacterial enzymes in the degree of preference for Q-5′MP over Q *in vitro* (12-fold versus 1.7-fold, respectively) may reflect different degrees of direct utilization of Q *in vivo* by different species. Nonetheless, the collective evidence indicates that Q-5′MP, not Q, is the biologically relevant substrate of *Hs*QNG1 and is an intermediate in the q salvage pathway. This intermediate may be generated by a cellular kinase. Based on previous observations that crude extracts of Vero cells contain a q salvage activity when supplied with Q, but the membrane-free extracts do not (30), we suspect that this putative kinase may be membrane associated. QNG1 may also recycle q from intracellular Q-5′MP pools generated by degradation of Q-containing tRNAs via the rapid tRNA decay pathway, which includes processive 5′-to-3′ RNases that produce 5′-mononucleotides (66–68). The tight architecture of the queuine binding pocket of Qng1/QNG1 is consistent with its selectivity for queuine-containing substrates (Figure 4F, Supplementary Figure S9e–h). Such specificity would be critical for an organism's ability to salvage this micronutrient.

Qng1/QNG1 is the second known N-glycosylase that is specific for the queuine base, next to the recently discovered Q nucleoside hydrolase QueK, involved in q salvage in the enteropathogen *C. difficile* (69). The two enzymes are unrelated in structure and mechanism. Qng1 adopts an HhH-glycosylase fold, prefers Q-5′MP as substrate, is metal independent and functions as a monomer; while QueK is a homotrimeric protein with a preference for Q as substrate and belongs to the Ca^{2+}-dependent nucleoside hydrolase (NH) superfamily which use a Rossmann-fold catalytic core and a bound Ca^{2+} ion to coordinate the substrate ribose and nucleophilic water molecule (single-displacement mechanism) (70). Further, Qng1 is structurally distinct from all known nucleotide hydrolases, which are all Rossmann fold-containing multimeric proteins, including the ppnN family of pyrimidine/purine-5′-nucleotide nucleosidases (71), the LOG family of cytokinin riboside-5′-monophosphate phosphoribohydrolases (72), 2′-deoxyguanosine-5′-monophosphate hydrolase DNPH1 (73), and cytosine-5′-monophosphate hydrolase Blsm (74) and hydroxyl-methyl cytosine-5′-monophosphate hydrolase MilB (75) involved in the biosynthesis of the peptidyl nucleoside antifungal agents blasticidin and mildiomycin, respectively.

The prevalence of Qng1/QNG1 across species, coincident with a non-redundant and highly specific catalytic function in Q-5′MP hydrolysis, highlights both an essential and specialized role for this family of enzymes in queuine salvage. This has functional consequences for optimal cellular activity since deficiencies in queuine can negatively impact the speed and accuracy of cytosolic and mitochondrial protein translation, trigger endoplasmic reticulum stress and activate the unfolded protein response (76–79). Consistent with these cellular functions, queuine and its analogues have been shown to avert disease mechanisms associated with neurodegeneration (16) and autoimmunity (24), leading to queuine being marketed as a key nutrient for aging and health (80). The greater molecular, cellular, and functional understanding of the Qng1/QNG1 family provided here, opens yet further possibilities to interrogate this ancient and intriguing RNA modification pathway.

DATA AVAILABILITY

Atomic coordinates and structure factors for C-terminally His$_6$-tagged *St*Qng1 apo structure (SeMet structure), wild-type (active, C-terminal His$_6$ tag removed) *St*Qng1 apo form, C-terminally His$_6$-tagged *St*Qng1 bound to Q, C-terminally His$_6$-tagged *St*Qng1 bound to Q-5′MP, C-terminally His$_6$-tagged *St*Qng1 K199C mutant bound to Q, and wild-type (active, C-terminal His$_6$ tag removed) human QNG1 in complex with q have been deposited with the Protein Data Bank under accession numbers 7U07, 7UK3, 7U1O, 7U91, 7U5A and 8DL3, respectively, and are publicly available as of the date of publication.

SUPPLEMENTARY DATA

Supplementary Data are available at NAR Online.

REFERENCES

1. Fergus,C., Barnes,D., Alqasem,M.A. and Kelly,V.P. (2015) The queuine micronutrient: charting a course from microbe to man. *Nutrients*, **7**, 2897–2929.

2. Kasai,H., Ohashi,Z., Harada,F., Nishimura,S., Oppenheimer,N.J., Crain,P.F., Liehr,J.G., von Minden,D.L. and McCloskey,J.A. (1975) Structure of the modified nucleoside Q isolated from *Escherichia coli* transfer ribonucleic acid. 7-(4,5-cis-dihydroxy-1-cyclopenten-3-ylaminomethyl)-7-deazaguanosine. *Biochemistry*, **14**, 4198–4208.

3. Ohgi,T., Kondo,T. and Goto,T. (1979) Total synthesis of optically pure nucleoside Q. Determination of absolute configuration of natural nucleoside Q. *J. Am. Chem. Soc.*, **101**, 3629–3633.

4. Hutinet,G., Swairjo,M.A. and de Crécy-Lagard,V. (2017) Deazaguanine derivatives, examples of crosstalk between RNA and DNA modification pathways. *RNA Biol.*, **14**, 1175–1184.

5. Randerath,E., Agrawal,H.P. and Randerath,K. (1984) Specific lack of the hypermodified nucleoside, queuosine, in hepatoma mitochondrial aspartate transfer RNA and its possible biological significance. *Cancer Res.*, **44**, 1167–1171.

6. Mörl,M., Dörner,M. and Pääbo,S. (1995) C to U editing and modifications during the maturation of the mitochondrial tRNA(Asp) in marsupials. *Nucleic Acids Res.*, **23**, 3380–3384.

7. Fergus,C., Al-Qasem,M., Cotter,M., McDonnell,C.M., Sorrentino,E., Chevot,F., Hokamp,K., Senge,M.O., Southern,J.M., Connon,S.J. et al. (2021) The human tRNA-guanine transglycosylase displays promiscuous nucleobase preference but strict tRNA specificity. *Nucleic Acids Res.*, **49**, 4877–4890.

8. Crain,P.F., Sethi,S.K., Katze,J.R. and McCloskey,J.A. (1980) Structure of an amniotic fluid component, 7-(4,5-cis-dihydroxy-1-cyclopenten-3-ylaminomethyl)-7-deazaguanine (queuine), a substrate for tRNA: guanine transglycosylase. *J. Biol. Chem.*, **255**, 8405–8407.

9. Okada,N. and Nishimura,S. (1977) Enzymatic synthesis of Q* nucleoside containing mannose in the anticodon of tRNA: isolation of a novel mannosyltransferase from a cell-free extract of rat liver. *Nucleic Acids Res.*, **4**, 2931–2937.

10. Kasai,H., Nakanishi,K., Macfarlane,R.D., Torgerson,D.F., Ohashi,Z., McCloskey,J.A., Gross,H.J. and Nishimura,S. (1976) Letter: the structure of Q* nucleoside isolated from rabbit liver transfer ribonucleic acid. *J. Am. Chem. Soc.*, **98**, 5044–5046.

11. Okada,N., Shindo-Okada,N. and Nishimura,S. (1977) Isolation of mammalian tRNA[Asp] and tRNA[Tyr] by lectin-Sepharose affinity column chromatography. *Nucleic Acids Res.*, **4**, 415–423.

12. Rakovich,T., Boland,C., Bernstein,I., Chikwana,V.M., Iwata-Reuyl,D. and Kelly,V.P. (2011) Queuosine deficiency in eukaryotes compromises tyrosine production through increased tetrahydrobiopterin oxidation. *J. Biol. Chem.*, **286**, 19354–19363.

13. Skolnick,S.D. and Greig,N.H. (2019) Microbes and monoamines: potential neuropsychiatric consequences of dysbiosis. *Trends Neurosci.*, **42**, 151–163.

14. Siard,T.J., Katze,J.R. and Farkas,W.R. (1989) Queuine is incorporated into brain transfer RNA. *Neurochem. Res.*, **14**, 1159–1164.

15. Marks,T. and Farkas,W.R. (1997) Effects of a diet deficient in tyrosine and queuine on germfree mice. *Biochem. Biophys. Res. Commun.*, **230**, 233–237.

16. Richard,P., Kozlowski,L., Guillorit,H., Garnier,P., McKnight,N.C., Danchin,A. and Manière,X. (2021) Queuine, a bacterial-derived hypermodified nucleobase, shows protection in *in vitro* models of neurodegeneration. *PLoS One*, **16**, e0253216.

17. Hayes,P., Fergus,C., Ghanim,M., Cirzi,C., Burtnyak,L., McGrenaghan,C.J., Tuorto,F., Nolan,D.P. and Kelly,V.P. (2020) Queuine micronutrient deficiency promotes Warburg metabolism and reversal of the mitochondrial ATP synthase in HeLa cells. *Nutrients*, **12**, 871.

18. Reisser,T., Langgut,W. and Kersten,H. (1994) The nutrient factor queuine protects HeLa cells from hypoxic stress and improves metabolic adaptation to oxygen availability. *Eur. J. Biochem.*, **221**, 979–986.

19. Kulkarni,S., Rubio,M.A.T., Hegedűsová,E., Ross,R.L., Limbach,P.A., Alfonzo,J.D. and Paris,Z. (2021) Preferential import of queuosine-modified tRNAs into *Trypanosoma brucei* mitochondrion is critical for organellar protein synthesis. *Nucleic Acids Res.*, **49**, 8247–8260.

20. White,B.N., Tener,G.M., Holden,J. and Suzuki,D.T. (1973) Activity of a transfer RNA modifying enzyme during the development of *Drosophila* and its relationship to the *su(s)* locus. *J. Mol. Biol.*, **74**, 635–651.

21. Dirheimer,G., Baranowski,W. and Keith,G. (1995) Variation in tRNA modifications, particularly of their queuine content in higher eukaryotes. Its relation to malignancy grading. *Biochimie*, **77**, 99–103.

22. Baranowski,W., Dirheimer,G., Jakowicki,J.A. and Keith,G. (1994) Deficiency of queuine, a highly modified purine base, in transfer RNAs from primary and metastatic ovarian malignant tumors in women. *Cancer Res.*, **54**, 4468–4471.

23. Huang,B.S., Wu,R.T. and Chien,K.Y. (1992) Relationship of the queuine content of tRNA to histopathological grading and survival in human lung cancer. *Cancer Res.*, **52**, 4696–4700.

24. Varghese,S., Cotter,M., Chevot,F., Fergus,C., Cunningham,C., Mills,K.H., Connon,S.J., Southern,J.M. and Kelly,V.P. (2017) *In vivo* modification of tRNA with an artificial nucleobase leads to full disease remission in an animal model of multiple sclerosis. *Nucleic Acids Res.*, **45**, 2029–2039.

25. Morris,R.C. and Elliott,M.S. (2001) Queuosine modification of tRNA: a case for convergent evolution. *Mol. Genet. Metab.*, **74**, 147–159.

26. Stengl,B., Reuter,K. and Klebe,G. (2005) Mechanism and substrate specificity of tRNA-guanine transglycosylases (TGTs): tRNA-modifying enzymes from the three different kingdoms of life share a common catalytic mechanism. *ChemBioChem*, **6**, 1926–1939.

27. Sievers,K., Welp,L., Urlaub,H. and Ficner,R. (2021) Structural and functional insights into human tRNA guanine transgylcosylase. *RNA Biol.*, **18**, 382–396.

28. Shaheen,R., Han,L., Faqeih,E., Ewida,N., Alobeid,E., Phizicky,E.M. and Alkuraya,F.S. (2016) A homozygous truncating mutation in PUS3 expands the role of tRNA modification in normal cognition. *Hum. Genet.*, **135**, 707–713.

29. Elliott,M.S., Trewyn,R.W. and Katze,J.R. (1985) Inhibition of queuine uptake in cultured human fibroblasts by phorbol-12,13-didecanoate. *Cancer Res.*, **45**, 1079–1085.

30. Gündüz,U. and Katze,J.R. (1984) Queuine salvage in mammalian cells. Evidence that queuine is generated from queuosine 5'-phosphate. *J. Biol. Chem.*, **259**, 1110–1113.

31. Katze,J.R., Gündüz,U., Smith,D.L., Cheng,C.S. and McCloskey,J.A. (1984) Evidence that the nucleic acid base queuine is incorporated intact into tRNA by animal cells. *Biochemistry*, **23**, 1171–1176.

32. Gündüz,U. and Katze,J.R. (1982) Salvage of the nucleic acid base queuine from queuine-containing TRNA by animal cells. *Biochem. Biophys. Res. Commun.*, **109**, 159–167.

33. Kirtland,G.M., Morris,T.D., Moore,P.H., O'Brian,J.J., Edmonds,C.G., McCloskey,J.A. and Katze,J.R. (1988) Novel salvage of queuine from queuosine and absence of queuine synthesis in *Chlorella pyrenoidosa* and *Chlamydomonas reinhardtii*. *J. Bacteriol.*, **170**, 5633–5641.

34. Zallot,R., Brochier-Armanet,C., Gaston,K.W., Forouhar,F., Limbach,P.A., Hunt,J.F. and de Crécy-Lagard,V. (2014) Plant, animal, and fungal micronutrient queuosine is salvaged by members of the DUF2419 protein family. *ACS Chem. Biol.*, **9**, 1812–1825.

35. Ohi,Y., Qin,H., Hong,C., Blouin,L., Polo,J.M., Guo,T., Qi,Z., Downey,S.L., Manos,P.D., Rossi,D.J. et al. (2011) Incomplete DNA methylation underlies a transcriptional memory of somatic cells in human iPS cells. *Nat. Cell Biol.*, **13**, 541–549.

36. Sweetser,D.A., Peniket,A.J., Haaland,C., Blomberg,A.A., Zhang,Y., Zaidi,S.T., Dayyani,F., Zhao,Z., Heerema,N.A., Boultwood,J. et al. (2005) Delineation of the minimal commonly deleted segment and identification of candidate tumor-suppressor genes in del(9q) acute myeloid leukemia. *Genes Chromosomes Cancer*, **44**, 279–291.

37. Patel,B.I., Heiss,M., Samel-Pommerencke,A., Carell,T. and Ehrenhofer-Murray,A.E. (2022) Queuosine salvage in fission yeast by Qng1-mediated hydrolysis to queuine. *Biochem. Biophys. Res. Commun.*, **624**, 146–150.

38. Sarid,L., Sun,J., Chittrakanwong,J., Trebicz-Geffen,M., Ye,J., Dedon,P.C. and Ankri,S. (2022) Queuine salvaging in the human parasite *Entamoeba histolytica*. *Cells*, **11**, 2509.

39. Kim,D.U., Hayles,J., Kim,D., Wood,V., Park,H.O., Won,M., Yoo,H.S., Duhig,T., Nam,M., Palmer,G. et al. (2010) Analysis of a genome-wide set of gene deletions in the fission yeast *Schizosaccharomyces pombe*. *Nat. Biotechnol.*, **28**, 617–623.

40. Doublie,S. (1997) Preparation of selenomethionyl proteins for phase determination. *Methods Enzymol.*, **276**, 523–530.

41. Minor,W., Cymborowski,M., Otwinowski,Z. and Chruszcz,M. (2006) HKL-3000: the integration of data reduction and structure

solution–from diffraction images to an initial model in minutes. *Acta Crystallogr. D Biol. Crystallogr.*, **62**, 859–866.

42. Kabsch,W. (2010) XDS. *Acta Crystallogr. D*, **66**, 125–132.

43. Adams,P.D., Afonine,P.V., Bunkoczi,G., Chen,V.B., Davis,I.W., Echols,N., Headd,J.J., Hung,L.W., Kapral,G.J., Grosse-Kunstleve,R.W. *et al.* (2010) PHENIX: a comprehensive Python-based system for macromolecular structure solution. *Acta Crystallogr. D Biol. Crystallogr.*, **66**, 213–221.

44. Adams,P.D., Gopal,K., Grosse-Kunstleve,R.W., Hung,L.W., Ioerger,T.R., McCoy,A.J., Moriarty,N.W., Pai,R.K., Read,R.J., Romo,T.D. *et al.* (2004) Recent developments in the PHENIX software for automated crystallographic structure determination. *J. Synchrotron Radiat.*, **11**, 53–55.

45. McCoy,A.J., Grosse-Kunstleve,R.W., Adams,P.D., Winn,M.D., Storoni,L.C. and Read,R.J. (2007) Phaser crystallographic software. *J. Appl. Crystallogr.*, **40**, 658–674.

46. Terwilliger,T. (2004) SOLVE and RESOLVE: automated structure solution, density modification and model building. *J. Synchrotron Radiat.*, **11**, 49–52.

47. Terwilliger,T.C., Grosse-Kunstleve,R.W., Afonine,P.V., Moriarty,N.W., Zwart,P.H., Hung,L.W., Read,R.J. and Adams,P.D. (2008) Iterative model building, structure refinement and density modification with the PHENIX AutoBuild wizard. *Acta Crystallogr. D Biol. Crystallogr.*, **64**, 61–69.

48. Afonine,P.V., Grosse-Kunstleve,R.W., Echols,N., Headd,J.J., Moriarty,N.W., Mustyakimov,M., Terwilliger,T.C., Urzhumtsev,A., Zwart,P.H. and Adams,P.D. (2012) Towards automated crystallographic structure refinement with phenix.refine. *Acta Crystallogr. D Biol. Crystallogr.*, **68**, 352–367.

49. Emsley,P., Lohkamp,B., Scott,W.G. and Cowtan,K. (2010) Features and development of Coot. *Acta Crystallogr. D Biol. Crystallogr.*, **66**, 486–501.

50. Murshudov,G.N., Skubak,P., Lebedev,A.A., Pannu,N.S., Steiner,R.A., Nicholls,R.A., Winn,M.D., Long,F. and Vagin,A.A. (2011) REFMAC5 for the refinement of macromolecular crystal structures. *Acta Crystallogr. D Biol. Crystallogr.*, **67**, 355–367.

51. Winn,M.D., Ballard,C.C., Cowtan,K.D., Dodson,E.J., Emsley,P., Evans,P.R., Keegan,R.M., Krissinel,E.B., Leslie,A.G., McCoy,A. *et al.* (2011) Overview of the CCP4 suite and current developments. *Acta Crystallogr. D Biol. Crystallogr.*, **67**, 235–242.

52. Jumper,J., Evans,R., Pritzel,A., Green,T., Figurnov,M., Ronneberger,O., Tunyasuvunakool,K., Bates,R., Žídek,A., Potapenko,A. *et al.* (2021) Highly accurate protein structure prediction with AlphaFold. *Nature*, **596**, 583–589.

53. Phillips,G., Swairjo,M.A., Gaston,K.W., Bailly,M., Limbach,P.A., Iwata-Reuyl,D. and de Crecy-Lagard,V. (2012) Diversity of archaeosine synthesis in crenarchaeota. *ACS Chem. Biol.*, **7**, 300–305.

54. Igloi,G.L. and Kössel,H. (1985) Affinity electrophoresis for monitoring terminal phosphorylation and the presence of queuosine in RNA. Application of polyacrylamide containing a covalently bound boronic acid. *Nucleic Acids Res.*, **13**, 6881–6898.

55. Lingaraju,G.M., Sartori,A.A., Kostrewa,D., Prota,A.E., Jiricny,J. and Winkler,F.K. (2005) A DNA glycosylase from *Pyrobaculum aerophilum* with an 8-oxoguanine binding mode and a noncanonical helix-hairpin-helix structure. *Structure*, **13**, 87–98.

56. Bruner,S.D., Norman,D.P. and Verdine,G.L. (2000) Structural basis for recognition and repair of the endogenous mutagen 8-oxoguanine in DNA. *Nature*, **403**, 859–866.

57. Sarre,A., Ökvist,M., Klar,T., Hall,D.R., Smalås,A.O., McSweeney,S., Timmins,J. and Moe,E. (2015) Structural and functional characterization of two unusual endonuclease III enzymes from *Deinococcus radiodurans*. *J. Struct. Biol.*, **191**, 87–99.

58. Brooks,S.C., Adhikary,S., Rubinson,E.H. and Eichman,B.F. (2013) Recent advances in the structural mechanisms of DNA glycosylases. *Biochim. Biophys. Acta*, **1834**, 247–271.

59. Dalhus,B., Forsbring,M., Helle,I.H., Vik,E.S., Forstrøm,R.J., Backe,P.H., Alseth,I. and Bjørås,M. (2011) Separation-of-function mutants unravel the dual-reaction mode of human 8-oxoguanine DNA glycosylase. *Structure*, **19**, 117–127.

60. Hashimoto,H., Zhang,X. and Cheng,X. (2012) Excision of thymine and 5-hydroxymethyluracil by the MBD4 DNA glycosylase domain:

61. Hollis,T., Ichikawa,Y. and Ellenberger,T. (2000) DNA bending and a flip-out mechanism for base excision by the helix-hairpin-helix DNA glycosylase, *Escherichia Coli AlkA*. *EMBO J.*, **19**, 758–766.

62. Woods,R.D., O'Shea,V.L., Chu,A., Cao,S., Richards,J.L., Horvath,M.P. and David,S.S. (2016) Structure and stereochemistry of the base excision repair glycosylase MutY reveal a mechanism similar to retaining glycosidases. *Nucleic Acids Res.*, **44**, 801–810.

63. Werner,R.M. and Stivers,J.T. (2000) Kinetic isotope effect studies of the reaction catalyzed by uracil DNA glycosylase: evidence for an oxocarbenium ion-uracil anion intermediate. *Biochemistry*, **39**, 14054–14064.

64. McCann,J.A. and Berti,P.J. (2008) Transition-state analysis of the DNA repair enzyme MutY. *J. Am. Chem. Soc.*, **130**, 5789–5797.

65. Pidugu,L.S., Bright,H., Lin,W.-J., Majumdar,C., Van Ostrand,R.P., David,S.S., Pozharski,E. and Drohat,A.C. (2021) Structural insights into the mechanism of base excision by MBD4. *J. Mol. Biol.*, **433**, 167097.

66. Hopper,A.K. (1998) Nuclear functions charge ahead. *Science*, **282**, 2003–2004.

67. Stevens,A. (1980) Purification and characterization of a *Saccharomyces cerevisiae* exoribonuclease which yields 5'-mononucleotides by a 5' leads to 3' mode of hydrolysis. *J. Biol. Chem.*, **255**, 3080–3085.

68. Chernyakov,I., Whipple,J.M., Kotelawala,L., Grayhack,E.J. and Phizicky,E.M. (2008) Degradation of several hypomodified mature tRNA species in *Saccharomyces cerevisiae* is mediated by Met22 and the 5'-3' exonucleases Rat1 and Xrn1. *Genes Dev.*, **22**, 1369–1380.

69. Yuan,Y., Zallot,R., Grove,T.L., Payan,D.J., Martin-Verstraete,I., Šepić,S., Balamkundu,S., Neelakandan,R., Gadi,V.K., Liu,C.-F. *et al.* (2019) Discovery of novel bacterial queuine salvage enzymes and pathways in human pathogens. *Proc. Natl. Acad. Sci. U.S.A.*, **116**, 19126–19135.

70. Versées,W. and Steyaert,J. (2003) Catalysis by nucleoside hydrolases. *Curr. Opin. Struct. Biol.*, **13**, 731–738.

71. Zhang,Y.E., Bærentsen,R.L., Fuhrer,T., Sauer,U., Gerdes,K. and Brodersen,D.E. (2019) (p)ppGpp regulates a bacterial nucleosidase by an allosteric two-domain switch. *Mol. Cell*, **74**, 1239–1249.

72. Seo,H., Kim,S., Sagong,H.Y., Son,H.F., Jin,K.S., Kim,I.K. and Kim,K.J. (2016) Structural basis for cytokinin production by LOG from *Corynebacterium glutamicum*. *Sci. Rep.*, **6**, 31390.

73. Yang,Y., Padilla,A., Zhang,C., Labesse,G. and Kaminski,P.A. (2009) Structural characterization of the mammalian deoxynucleotide N-hydrolase Rcl and its stabilizing interactions with two inhibitors. *J. Mol. Biol.*, **394**, 435–447.

74. Kang,M., Doddapaneni,K., Sarni,S., Heppner,Z., Wysocki,V. and Wu,Z. (2020) Solution structure of the nucleotide hydrolase BlsM: implication of its substrate specificity. *Protein Sci.*, **29**, 1760–1773.

75. Zhao,G., Wu,G., Zhang,Y., Liu,G., Han,T., Deng,Z. and He,X. (2014) Structure of the N-glycosidase MilB in complex with hydroxymethyl CMP reveals its Arg23 specifically recognizes the substrate and controls its entry. *Nucleic Acids Res.*, **42**, 8115–8124.

76. Suzuki,T., Yashiro,Y., Kikuchi,I., Ishigami,Y., Saito,H., Matsuzawa,I., Okada,S., Mito,M., Iwasaki,S., Ma,D. *et al.* (2020) Complete chemical structures of human mitochondrial tRNAs. *Nat. Commun.*, **11**, 4269.

77. Müller,M., Legrand,C., Tuorto,F., Kelly,V.P., Atlasi,Y., Lyko,F. and Ehrenhofer-Murray,A.E. (2019) Queuine links translational control in eukaryotes to a micronutrient from bacteria. *Nucleic Acids Res.*, **47**, 3711–3727.

78. Tuorto,F., Legrand,C., Cirzi,C., Federico,G., Liebers,R., Müller,M., Ehrenhofer-Murray,A.E., Dittmar,G., Gröne,H.J. and Lyko,F. (2018) Queuosine-modified tRNAs confer nutritional control of protein translation. *EMBO J.*, **37**, e99777.

79. Zaborske,J.M., DuMont,V.L., Wallace,E.W., Pan,T., Aquadro,C.F. and Drummond,D.A. (2014) A nutrient-driven tRNA modification alters translational fidelity and genome-wide protein coding across an animal genus. *PLoS Biol.*, **12**, e1002015.

80. Ames,B.N. (2018) Prolonging healthy aging: longevity vitamins and proteins. *Proc. Natl. Acad. Sci. U.S.A.*, **115**, 10836–10844.